Available online at www.sciencedirect.com
SCIENCE DIRECT
International Journal of Mass Spectrometry 253 (2006) 288–304
International Journal of Mass Spectrometry
www.elsevier.com/locate/ijms

Sequential bond energies of water to sodium proline cation

S.J. Ye, R.M. Moision, P.B. Armentrout *

Department of Chemistry, University of Utah, Salt Lake City, UT 84112, United States

Received 14 March 2006; received in revised form 10 May 2006; accepted 10 May 2006
Available online 6 June 2006

Abstract

Absolute bond dissociation energies of water to sodium proline cations and proline to hydrated sodium cations are determined experimentally by collision-induced dissociation of $Na^+Pro(H_2O)_x$, where $x = 1$–4, complexes with xenon in a guided ion beam mass spectrometer. Experimental results show that the binding energies of water and proline to the complexes decrease monotonically with increasing number of water molecules. Ab initio calculations at three different levels show reasonable agreement with the experimental bond energies of water and proline for $x = 1$–4 except the theoretical values are higher for losing proline from $x = 3$ and 4. The primary binding site for Na^+ is at the C terminus of proline for $x = 0$–4, i.e., the solvated sodiated proline complexes are in their zwitterionic forms. Calculations suggest that the first solvent shell of Na^+Pro is essentially complete at four waters.

Keywords: Guided ion beam mass spectrometry; Sodium proline cation; Bond dissociation energies; Solvation energies

1. Introduction

Alkali metals are known to play an important role in biological systems, including modulating enzyme activity [1]. The structures of biological macromolecules in solution are stabilized by their interactions with water and their counter ions, such as Na^+ and K^+ [2,3]. The overall thermodynamic outcome of all the multitude of interactions potentially can be understood by careful examination of the intrinsic interactions on a pairwise basis. Gas-phase studies provide a means to quantitatively assess these interactions in systems small enough for meaningful comparisons to theory.

The binding affinities of alkali metal cations with amino acids, small peptides, and their analogues have been studied extensively in the past decade both experimentally and theoretically [4–16]. These interactions are mainly electrostatic and therefore the strength decreases with increasing size of the alkali metal ion [17]. The binding affinity between them can also be strengthened by chelation with amino acids and peptide side chains [18]. However, much less work exists for interactions of these biological systems when solvated with water. William's group investigated the hydration of metalated valine using blackbody infrared radiative dissociation (BIRD). They find that the interaction between water and metalated valine also decreases with the size of the alkali metal ion. They reported first and second water room temperature binding energies of 85 and 58–61 kJ/mol to Li^+Val, 66 and 52 kJ/mol to Na^+Val, and a second water binding energy of 31 kJ/mol to K^+Val systems, respectively [19–22]. In our laboratory, threshold collision-induced dissociation (TCID) experiments were used to determine the monotonic decrease of water binding energies (75, 55, 40, 32 kJ/mol) with increasing number of water molecules for the $Na^+Gly(H_2O)_x$ system, $x = 1$–4 [23]. Because valine and glycine are both aliphatic or hydrophobic amino acids, they behave similarly in the gas phase when ionized by a sodium ion, leading to comparable water binding energies. The sodium ion favors [N,CO] coordination to nonzwitterionic valine and glycine, but changes to CO coordination when hydrated by two or more water molecules [4,19,21,23]. The hydrated sodium valine and glycine systems calculations show that their lowest energy structures still favor charge solvated structure up to three and four water molecules, respectively, whereas a zwitterionic form is favored in aqueous solution.

Recently, systems involving proline have drawn attention because of its unique structure containing a structurally rigid five-member ring that hinders torsional motions and a secondary amine group that makes it more basic than most other amino acids. Thus experiments and calculations show that sodium

* Corresponding author. Tel.: +1 801 581 7885; fax: +1 801 581 8433.
E-mail address: armentrout@chem.utah.edu (P.B. Armentrout).

1387-3806/$ – see front matter © 2006 Elsevier B.V. All rights reserved.
doi:10.1016/j.ijms.2006.05.008

cation binds to the carboxylate acid group of zwitterionic proline [11,12,15,24]. Williams and co-workers recently investigated the hydration of sodiated proline analogues [25]. They determined the first water binding energy to sodiated α-Me–Pro at 298 K to be 48 kJ/mol and concluded that the sodiated singly hydrated proline is also zwitterionic because the proton affinity of proline is 8 kJ/mol higher than that of α-Me–Pro. Their calculations show the water binds directly to the metal ion and makes no difference to the Na^+ (amino acid) structure. In the present studies, the absolute bond dissociation energies (BDEs) of water to sodium proline cation and proline to hydrated sodium cations are measured using competitive TCID methods. Complementary structural information about these systems is obtained by theoretical studies.

2. Experimental and computational section

2.1. General experimental procedures

The instrument used to measure the cross-sections for TCID of the hydrated sodium proline complexes is a guided ion beam tandem mass spectrometer (GIBMS), which has been described previously in detail [26,27]. Briefly, the instrument comprises five parts: ion source, momentum analyzer, collision region surrounding an octopole ion beam guide, quadrupole mass filter, and detector. Sodium ions are generated in the ion source using a continuous dc discharge where the cathode is a tantalum boat filled with sodium metal. Typical operating conditions of the discharge are 1.6–2.2 kV and 15–25 mA. The sodium cations produced are carried by a flow of buffer gas (∼10% Ar in He) through a 1 m long flow tube at a rate of 4000–9000 standard cm^3/min, usually at a pressure of 0.4–0.9 Torr. At 10 cm downstream from the discharge, the neutral proline ligand is introduced using a temperature controllable heated probe (145–180 °C). Water is then introduced about 50 cm from the discharge. The complex ions of interest are formed via three-body associative reactions of Na^+ with the proline and water ligands in the flow of He/Ar. The complex ions are thermalized to 300 K (the temperature of the flow tube) both vibrationally and rotationally by undergoing $\sim 10^5$ collisions with the buffer gases in the 1 m long flow tube [28–31]. Therefore, the rovibrational internal energies of all complex ions when exiting the flow tube can be described by a Maxwell–Boltzmann distribution at 300 K. After exiting the flow tube, the ionic complexes are focused through two differentially pumped regions, accelerated, and focused into a 66° magnetic momentum analyzer that acts as a mass selector. The resulting mass-selected ion beam, $Na^+Pro(H_2O)_x$, $x = 1$–4, is decelerated using an exponential retarder to a well-defined and variable kinetic energy and injected into a radio frequency double octopole ion beam guide region [27,32–34]. The neutral reactant (here, Xe) is introduced into a gas collision cell that surrounds the octopole. All unreacted complex ions as well as product ions formed by reactions with the neutral gas are trapped by the octopole in the radial direction. After drifting to the end of the octopole, all ions are extracted and focused into a quadrupole mass filter for mass analysis. Ions are efficiently detected with a 27 kV conversion dynode-secondary electron scintillation detector interfaced with fast pulse counting electronics [35].

Ions intensities, measured as a function of collision energy, are converted to absolute cross-sections as described previously [32]. The absolute uncertainties in cross-section magnitudes are estimated to be ±20% and the relative uncertainties are approximately ±5%. Laboratory (lab) energies are converted to center-of-mass (CM) energies using the equation $E_{CM} = E_{lab} \times M/(M+m)$, where M and m are the neutral and ion masses, respectively. All energies cited below are in the CM frame unless otherwise noted. The absolute energy scale and the corresponding full width at half-maximum (FWHM) of the ion beam kinetic energy distribution are determined by using the octopole as a retarding energy analyzer [32]. The energy spread is nearly Gaussian and has a typical FWHM of 0.2–0.4 eV (lab) in the present experiments.

It has been shown previously that the pressure of the neutral reactant can influence the shape of TCID cross-sections because of the effects of multiple collisions [36]. At sufficiently low pressure, the cross-sections are independent of the measured pressure [32]. In the present systems, we observe a slight dependence on Xe pressure for the cross-section of the first dissociation product and an obvious dependence for the secondary and higher products. We attribute this to multiple energizing collisions that lead to an enhanced probability of dissociation. In order to obtain data free from pressure effects (i.e., at rigorously single collision conditions), we generally collect data at about 0.15, 0.08, and 0.04 mTorr, and the cross-sections are extrapolated to zero reactant pressure prior to threshold analysis, as described previously [36].

2.2. Dissociation threshold analysis

To determine threshold energies for endothermic reactions, cross-sections are modeled using Eq. (1),

$$\sigma(E) = \sigma_0 \sum_i \frac{g_i(E + E_i - E_0)^n}{E} \quad (1)$$

where σ_0 is an adjustable parameter that is energy independent, n another adjustable parameter that describes the energy deposition efficiency during collision [27], E is the relative kinetic energy, E_0 represents the CID threshold energy at 0 K, and the summation is over the rovibrational states I of the reactant ion having energies, E_i, and relative populations g_i, where $\sum g_i = 1$. Vibrational frequencies and rotational constants are taken from the ab initio calculations detailed in the next section. The Beyer–Swinehart algorithm [37] is used to evaluate the density of the rovibrational states and the relative populations g_i are calculated for a Maxwell–Boltzmann distribution at 300 K. In the present studies, two parallel dissociation channels compete with one another such that we use a variant of Eq. (1) that considers competitive CID, Eq. (2) as described in detail elsewhere [38].

$$\sigma_j(E) = \left(\frac{n\sigma_{0,j}}{E}\right) \sum g_i \int_{E_{0,j}-E_i}^{E} \left[\frac{k_j(E^*)}{k_{tot}(E^*)}\right] \{1 - e^{-k_{tot}(E^*)\tau}\} \times (E - \varepsilon)^{n-1}\, d(\varepsilon) \quad (2)$$

Here $\sigma_{0,j}$ is a scaling factor for channel j, $E_{0,j}$ the CID threshold at 0 K for channel j, τ the experimental time for dissociation ($\sim 5 \times 10^{-4}$ s in the extended dual octopole configuration as measured by time-of-flight studies [27]), ε the energy transferred from translation during the collision and E^* is the internal energy of the energized molecule (EM) after the collision, i.e., $E^* = \varepsilon + E_i$. The term $k_j(E^*)$ is the unimolecular rate constant for dissociation to channel j. This rate constant and $k_{tot}(E^*)$ are defined by Rice–Ramsperger–Kassel–Marcus (RRKM) theory as in Eq. (3) [39],

$$k_{tot}(E^*) = \sum_j k_j(E^*) = \sum_j \frac{d_j N_j^{\dagger}(E^* - E_{0,j})}{h\rho(E^*)} \quad (3)$$

where d_j is the reaction degeneracy, $N_j^{\dagger}(E* - E_{0,j})$ the sum of rovibrational states of the transition state (TS) for channel j at an energy $E^* - E_{0,j}$, and $\rho(E^*)$ is the density of states of the energized molecule (EM) at the available energy, E^*. In the limit that $k(E^*)$ is faster than the time-of-flight of the ions, the integration in Eq. (2) recovers Eq. (1).

Several effects that obscure the interpretation of the data must be accounted for during data analysis in order to produce accurate thermodynamic information. The first effect involves energy broadening resulting from the thermal motion of the neutral collision gas and the kinetic energy distribution of the reactant ion. This is accounted for by explicitly convoluting the model over both kinetic energy distributions, as described elsewhere in detail [32]. The second effect arises from the lifetime for dissociation. As the size of reactant molecules increases, so do the number of vibrational modes of the reactant ion and thus the time for energy randomization into the reaction coordinate after collision. At a certain point, some energized molecules may not dissociate during the time scale of the experiment [31]. This leads to a delayed onset for the CID threshold, a kinetic shift, which becomes more noticeable as the size of the molecule increases. These kinetic shifts are estimated by the incorporation of RRKM theory in Eq. (2), as described in detail elsewhere [40]. To evaluate the rate constants in Eq. (2), sets of rovibrational frequencies for the EM and all TSs are required. Because the metal–ligand interactions in $Na^+Pro(H_2O)_x$ are mainly electrostatic (ion–dipole, ion–quadrupole, and ion-induced dipole interactions), the most appropriate model for the TS is a loose association of the ion and neutral ligand fragments. Therefore, the TSs are treated as product-like, such that the TS frequencies are those of the dissociation products. The molecular parameters needed for the RRKM calculation are taken from the ab initio calculations detailed in the next section. The transitional frequencies are treated as rotors, a treatment that corresponds to a phase space limit (PSL), as described in detail elsewhere [38]. For $Na^+Pro(H_2O)_x$ complexes, the five transitional mode rotors have rotational constants equal to those of the $Na^+Pro(H_2O)_{x-1}$ and H_2O products or $Na^+(H_2O)_x$ and proline products. The 2D external rotations are treated adiabatically but with centrifugal effects included [41]. In the present work, the adiabatic 2D rotational energy is treated using a statistical distribution with an explicit summation over all the possible values of the rotational quantum number.

The model cross-section of Eq. (2) is convoluted with the kinetic energy distribution of the reactants and compared to the data. A nonlinear least-squares analysis is used to provide optimized values for $\sigma_{0,j}$, $E_{0,j}$, and n. The uncertainty associated with $E_{0,j}$ is estimated from the range of threshold values determined from different data sets with variations in vibrational frequencies (±10% and a factor of 2 for the M^+–L modes) and in the parameter n, variations in τ by a factor of 2, and the uncertainty in the absolute energy scale, 0.05 eV (lab).

In deriving the final optimized BDEs at 0 K, two assumptions are made. First, we assume that there is no activation barrier in excess of the reaction endothermicity for the loss of ligands, which is generally true for ion–molecule reactions, especially those such as the heterolytic bond cleavages considered here [42]. Second, the measured threshold $E_{0,j}$ for dissociation is from ground state reactant to ground state ion products and neutral ligands. Given the relatively long experimental time frame ($\sim 5 \times 10^{-4}$ s), dissociating products should be able to rearrange to their low energy conformations after collisional excitation.

2.3. Computational details

The systems we examine here have many low-lying conformations. A simulated annealing procedure using the AMBER program and the AMBER forcefield based on molecular mechanics [43] was used to search for possible stable structures in each system's conformational space. All possible structures identified in this way were further optimized using nwchem [44] at the HF/3-21G level [45,46]. Unique structures for each system that are within about 30 kJ/mol of the lowest energy structure (about 30 for each complex) were further optimized using Gaussian 03W [47] at the B3LYP/6-31G* level [48,49] with the "loose" keyword to facilitate more rapid convergence. The 10–15 lowest energy structures obtained from this procedure were then chosen for higher-level geometry optimizations and frequency calculations using density functional theory (DFT) at the B3LYP/6-311 + G** level [50,51]. When used in internal energy determinations or for RRKM calculations, the vibrational frequencies were scaled by 0.99 [52]. We have shown in previous work on the related $Na^+Gly(H_2O)_x$ systems that MP2(full) and B3LYP calculations using the same 6-31G** basis set gave almost identical structural and energy information [23]. Therefore, MP2(full)/6-311 + G** geometry optimizations were not performed for the present systems. Single point energy calculations were carried out for the lowest 6–15 of these optimized structures at the B3LYP, B3P86, and MP2(full) levels using the 6–311 + G(2d,2p) basis set [50]. Zero-point vibrational energy (ZPE) corrections were determined using scaled vibrational frequencies calculated at the B3LYP/6-311 + G** level. Basis set superposition errors (BSSE) for all single point energy calculations were estimated using the full counterpoise method in Gaussian 03W [47,53]. Previous work [4,23,54,55] has indicated that BSSE corrections on alkali metal systems are generally small for DFT calculations and we find this to be true here as well. Both B3LYP and B3P86 calculations have BSSE cor-

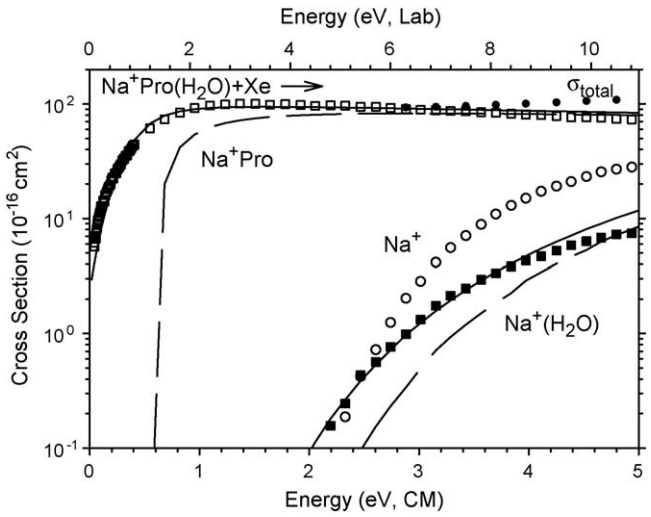

Fig. 1. Zero pressure extrapolated cross-section for CID of $Na^+Pro(H_2O)$ with Xe as a function of kinetic energy in the center-of-mass and laboratory frame. The solid lines show the model cross-section convoluted over the neutral and ion kinetic and internal energies. The dashed lines show the model cross-sections in the absence of experimental energy broadening for reactants with an internal energy of 0 K.

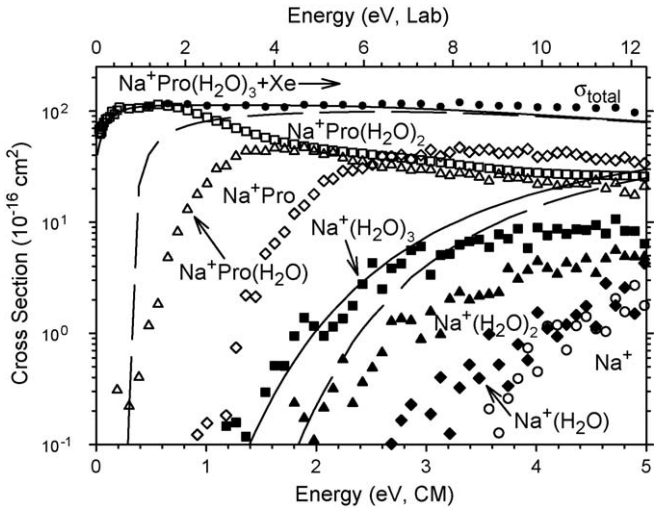

Fig. 3. Zero pressure extrapolated cross-section for CID of $Na^+Pro(H_2O)_3$ with Xe as a function of kinetic energy in the center-of-mass and laboratory frame. The solid lines show the model cross-section convoluted over the neutral and ion kinetic and internal energies. The dashed lines show the model cross-sections in the absence of experimental energy broadening for reactants with an internal energy of 0 K.

rections less than 5 kJ/mol whereas the MP2(full) values have BSSEs of 6–20 kJ/mol depending on the size of the molecule.

3. Results

3.1. Cross-sections for collision-induced dissociation

Experimental cross-sections were obtained for the interaction of Xe with $Na^+Pro(H_2O)_x$, $x = 1$–4. Figs. 1–4 show representative data for CID of these complexes. Over the energy ranges examined, the dominant dissociation process for all $Na^+Pro(H_2O)_x$ complexes is the loss of one water molecule in reaction (4).

$$Na^+Pro(H_2O)_x + Xe \rightarrow Na^+Pro(H_2O)_{x-1} + H_2O + Xe \quad (4)$$

The magnitudes of the cross-sections for losing one water molecule from $Na^+Pro(H_2O)_x$ increase from $x = 1$ to $x = 3$, whereas for $x = 4$, the cross-section is relatively small, which may indicate a different water binding pattern compared to $x = 1$–3. The primary cross-sections rise rapidly at low energy, level off, then generally decline at higher energies because of further dissociation of the primary product, as indicated by sub-

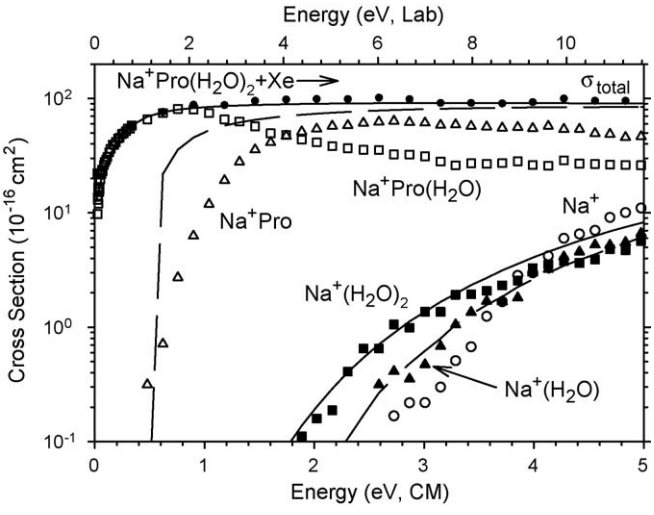

Fig. 2. Zero pressure extrapolated cross-section for CID of $Na^+Pro(H_2O)_2$ with Xe as a function of kinetic energy in the center-of-mass and laboratory frame. The solid lines show the model cross-section convoluted over the neutral and ion kinetic and internal energies. The dashed lines show the model cross-sections in the absence of experimental energy broadening for reactants with an internal energy of 0 K.

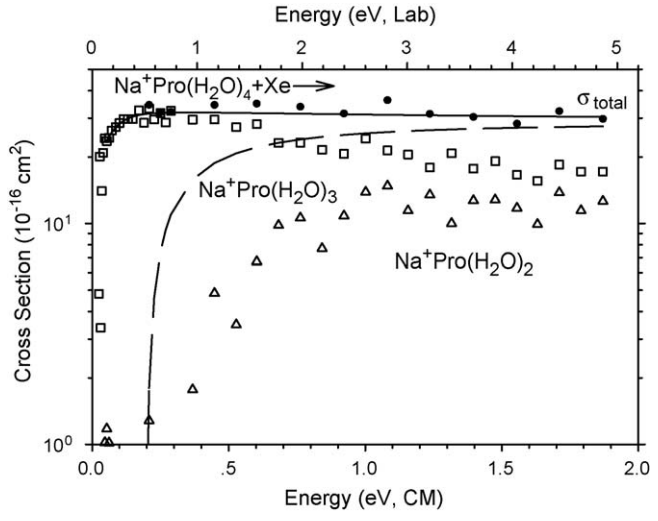

Fig. 4. Zero pressure extrapolated cross-section for CID of $Na^+Pro(H_2O)_4$ with Xe as a function of kinetic energy in the center-of-mass and laboratory frame. The solid lines show the model cross-section convoluted over the neutral and ion kinetic and internal energies. The dashed lines show the model cross-sections in the absence of experimental energy broadening for reactants with an internal energy of 0 K.

Table 1
Fitting parameters for Eq. (2) and entropies of activation at 1000 K[a]

Reactant	Ionic product	σ_0	n	E_0 (eV)	$\Delta S^{\ddagger}_{1000}$ (J/mol K)
Na^+Pro[b]	Na^+	15 (4)	1.40 (0.1)	1.93 (0.04)	30 (5)
$Na^+Pro(H_2O)$	Na^+Pro[c]	68 (28)	0.64 (0.11)	0.68 (0.05)	−9 (1)
	$Na^+(H_2O)$[c]	12 (4)		1.38 (0.09)	26 (1)
	Na^+Pro[d]	84 (30)	0.82 (0.10)	0.64 (0.05)	−9 (1)
	$Na^+(H_2O)$[d]	2 (1)	2.14 (0.14)	1.97 (0.17)	24 (2)
$Na^+Pro(H_2O)_2$	$Na^+Pro(H_2O)$[c]	99 (3)	1.00 (0.03)	0.46 (0.05)	39 (1)
	$Na^+(H_2O)_2$[c]	27 (6)		0.99 (0.07)	75 (2)
	$Na^+Pro(H_2O)$[d]	100 (2)	1.03 (0.04)	0.45 (0.06)	40 (1)
	$Na^+(H_2O)_2$[d]	3 (1)	2.76 (0.12)	1.78 (0.09)	73 (2)
$Na^+Pro(H_2O)_3$	$Na^+Pro(H_2O)_2$[c]	101 (14)	0.96 (0.07)	0.31 (0.04)	5(1)[e], −1(1)[f], 31 (1)[g]
	$Na^+(H_2O)_3$[c]	101 (14)		0.85 (0.05)	78(2)[e], 71(2)[f], 103(2)[g]
	$Na^+Pro(H_2O)_2$[d]	116 (7)	0.96 (0.02)	0.32 (0.04)	5(1)[e], −1(1)[f], 31 (1)[g]
	$Na^+(H_2O)_3$[d]	10 (2)	1.62 (0.23)	1.62 (0.12)	77(2)[e], 70(2)[f], 100(2)[g]
$Na^+Pro(H_2O)_4$	$Na^+Pro(H_2O)_3$	24 (8)	0.88 (0.19)	0.21 (0.06)	32 (2)

[a] Uncertainties are listed in parentheses.
[b] From Moison and Armentrout [24].
[c] Competitive fitting.
[d] Single channel fitting.
[e] Values obtained using 3W[bNH, bO$^-$]-ZW[CO]-C3u structure parameters. The listed σ_0, n, and E_0 values also utilize this structure, although the alternate structures yield nearly identical values.
[f] Values correspond to those from 3W[bO$^-$]-ZW[CO]-C3u.
[g] Values correspond to those from 3W[bO$^-$,bOH$_2$]-ZW[CO]-C3u.

sequent losses of water molecules to form $Na^+Pro(H_2O)_{x-y}$, $y = 2$ and 3. The absolute intensities of the ion beams were found to decrease with increasing solvation such that our sensitivity for CID of $Na^+Pro(H_2O)_4$ is rather poor, leading to the noisier cross-sections in Fig. 4.

In addition to reaction (4), loss of the proline ligand is observed in the competitive reaction (5) at higher energies in all cases except $x = 4$, where our sensitivity is reduced.

$$Na^+Pro(H_2O)_x + Xe \rightarrow Na^+(H_2O)_x + Pro + Xe \quad (5)$$

The $Na^+(H_2O)_x$ cross-sections are much smaller than those of the $Na^+Pro(H_2O)_{x-1}$ products and have apparent thresholds that are more than 1 eV higher. This indicates that the interaction between proline and Na^+ is stronger than that of H_2O and Na^+, consistent with previous measurements, $D_0(Na^+–Pro) = 186 \pm 4$ kJ/mol and $D_0(Na^+–H_2O) = 98 \pm 8$ kJ/mol [24,56]. Loss of water molecules from the $Na^+(H_2O)_x$ products were also found for $x = 1$–3. In no system was a ligand exchange process forming a Xe containing ion observed.

3.2. Threshold analysis and results

We have shown previously [24,38,57] that the best measurements of the thresholds for competitive dissociation processes come from the simultaneous analysis of the cross-sections. The apparent threshold for the higher energy process is elevated from its thermodynamic value because of competition with the lower energy channel. In the present $Na^+Pro(H_2O)_x$ systems, we carried out both simultaneous analysis and single channel analysis on these competitive processes with $x = 1$–3 for further comparison. The competitive model of Eq. (2) was used to analyze the competitive processes 4 and 5 for $Na^+Pro(H_2O)_x$ systems with $x = 1$–3 and the single channel cross-sections were modeled using Eq. (2) with only one channel ($k_j = k_{tot}$). For $Na^+Pro(H_2O)_4$, the weak ion intensity did not permit observation of the competitive channel, $Na^+(H_2O)_4$, therefore only the cross-section for losing water in process 4 was modeled. Figs. 1–4 show that all experimental cross-sections for reactions (4) and (5) are reproduced well by Eq. (2) over energy ranges of 1–3 eV. Eq. (2) with only one channel is able to reproduce the individual cross-sections for processes 4 and 5 over similar energy ranges with comparable fits to those shown in Figs. 1–4. The optimized parameters of Eq. (2) in both cases are reported in Table 1 along with results from previous work on CID of the Na^+Pro complex [24].

In previous studies of competitive dissociations [23,38,57], we found that independent scaling factors (different values of $\sigma_{0,j}$ for each channel) are sometimes needed in order to reproduce the experimental data when using the competitive analysis. The use of independent scaling factors compensates for neglected factors, such as reaction degeneracies, symmetry numbers of the reactant and product molecules, dipole moments of neutral products, and inaccurate estimations of metal–ligand frequencies, although all of these factors are included in the modeling to the best of our ability to estimate them. In the present study, independent scaling factors were used for $x = 1$ and 2 with relative $\sigma_{0,j}$ values of 5.7 and 3.7, respectively, whereas a common scaling factor could be used for $x = 3$ (Table 1).

The threshold values for losing water are almost unchanged no matter which method (competitive modeling or single chan-

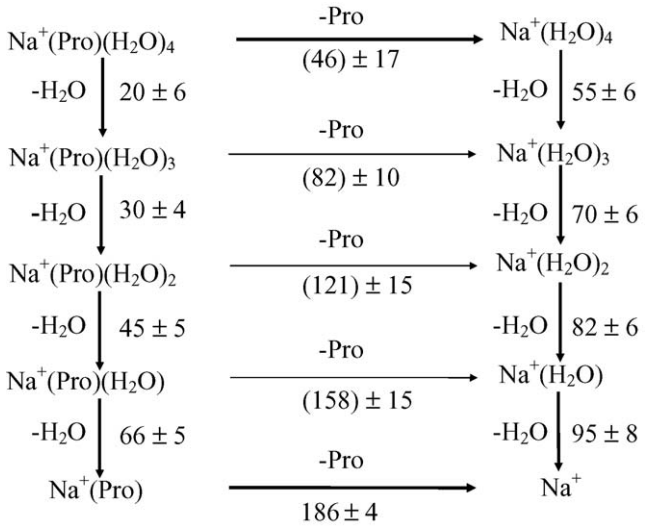

Fig. 5. Sequential hydration energies (kJ/mol) of Na^+ and Na^+(Pro) $D_0(Na^+–Pro)$ is taken from [24]. $D_0[(H_2O)_x\ Na^+–H_2O]$ values are from [55].

nel modeling) is used, as indicated in Table 1. However, the values for losing proline obtained using these two methods are very different from each other. For example, the E_0 value for losing proline from the $Na^+Pro(H_2O)$ complex using the single channel fitting method is even larger than the experimental E_0 value for losing proline from Na^+Pro [24]. This result clearly indicates that the E_0 values for the higher energy process 5 obtained by single channel modeling are elevated from their thermodynamic values because of the neglect of competition with the lower energy channel. Therefore, the E_0 values for losing proline obtained by single channel fitting can be treated as upper limits to the true thresholds.

For the competitive modeling results, the accuracy of the values can be checked by comparing to values obtained using a thermodynamic cycle, namely: $E_0[Na^+Pro(H_2O)_x \rightarrow Pro + Na^+(H_2O)_x] = E_0[Na^+Pro(H_2O)_x \rightarrow Na^+Pro + xH_2O] + E_0[Na^+Pro \rightarrow Pro + Na^+] - E_0[Na^+(H_2O)_x \rightarrow Na^+ + xH_2O]$ where the three E_0 values on the right of the equation have been independently measured either here or elsewhere [56]. This cycle is illustrated in Fig. 5, where starting with any complex on the left, the energy required to lose proline equals the energy of removing all the waters, then proline from Na^+Pro, then adding the waters back to bare Na^+. The results from these calculations are listed in Table 2 and compared with the threshold values obtained by competitive and single channel modeling. As concluded above, the single channel threshold values are well in excess of the thermodynamic cycle values with differences that gradually increase as x increases. In contrast, the competitive fitting thresholds for $x = 1$ and 2 are found to lie below the thermodynamic cycle values by 24 kJ/mol (close to the sum of the uncertainties in the two values), whereas the values for $x = 3$ are in reasonable agreement. As noted above, the competitive modeling results for losing proline from the $x = 1$ and 2 complexes required relative scaling factors of ~5.7 and 3.7, respectively, whereas the $x = 3$ complex could be analyzed using a common scaling factor. If a common scaling factor and thresholds obtained from the thermodynamic cycle are used to predict the results for $x = 1$ and 2, the predicted $Na^+(H_2O)_x$ cross-sections are smaller than the experimental results by factors of about 30. Thus, the competitive fit lowers the thresholds to increase the relative magnitude of these cross-sections. We can think of no statistical factors to include in our modeling that might be used to enhance the probability of the proline loss channel. Indeed, one might have anticipated that because the lowest energy channel for losing proline from these complexes requires changing from a zwitterionic structure (see discussion below) to neutral proline, reaction (5) would be less efficient than a statistical prediction. Likewise, if collection efficiency were a problem, the lighter $Na^+(H_2O)_x$ ions (which have larger velocities at the same energy) should be harder to collect than $Na^+Pro(H_2O)_{x-1}$.

Another indication that a statistical approach may not be adequate for the $Na^+Pro(H_2O)$ and $Na^+Pro(H_2O)_2$ complexes is the Na^+ cross-sections. For $Na^+Pro(H_2O)$, Fig. 1, the experimental cross-section for Na^+ is about twice as big as that of $Na^+(H_2O)$, which indicates that the Na^+ primarily comes from the primary Na^+Pro product ion. Likewise for $Na^+Pro(H_2O)_2$, Fig. 2, the Na^+ cross-section exceeds those for $Na^+(H_2O)$ and $Na^+(H_2O)_2$, whereas for $Na^+Pro(H_2O)_3$, Fig. 3, the Na^+ cross-section is the smallest of all products. Ultimately, we believe that the statistical competitive fitting model may begin to fail when the threshold difference between the two channels is too large. In such circumstances, the higher energy channel may not start until energies where dynamic effects begin to become important. Thus, competitive modeling worked well for $Na^+Gly(H_2O)_x$ because the Na^+Gly bond energy is weaker than that of Na^+Pro [23,24], and may work well for $Na^+Pro(H_2O)_3$ because the bond to proline

Table 2
Summary of E_0 (kJ/mol) for losing proline from $Na^+Pro(H_2O)_x$

Reactant	Single channel fit[a]	Competitive fit[b]	Cycle 1[c]	Cycle 2[d]	Average[e]
$Na^+Pro(H_2O)$	190 (17)	133 (9)	157 (10)	160 (12)	158 (15)
$Na^+Pro(H_2O)_2$	172 (9)	95 (7)	119 (13)	122 (9)	121 (15)
$Na^+Pro(H_2O)_3$	156 (12)	82 (5)	79 (15)	82 (5)	82 (10)
$Na^+Pro(H_2O)_4$	–	–	44 (17)	47 (10)	46 (17)

[a] Values from single channel modeling from Table 1.
[b] Values from competitive modeling from Table 1.
[c] Using $D_0(Na^+–Pro)$ as the reference value.
[d] Using $D_0(Na^+(H_2O)_3–Pro)$ as the reference value.
[e] Weighted average of cycle 1 and cycle 2. Uncertainties are two standard deviations of the mean.

has been weakened sufficiently by the addition of three water molecules.

On the basis of the good agreement between the $Na^+(H_2O)_3$–Pro bond energies obtained by competitive fitting and the thermodynamic cycle anchored by $D_0(Na^+–Pro)$, the former value can also be used as a reference value in a second thermodynamic cycle: $E_0[Na^+Pro(H_2O)_x \rightarrow Na^+(H_2O)_x + Pro] = E_0[Na^+Pro(H_2O)_x \rightarrow Na^+Pro(H_2O)_3 + (x-3)H_2O] + E_0[Na^+Pro(H_2O)_3 \rightarrow Na^+(H_2O)_3 + Pro] - E_0[Na^+(H_2O)_x \rightarrow Na^+(H_2O)_3 + (x-3)H_2O]$. These values along with the weighted average of the $Na^+(H_2O)_x$–Pro bond energies obtained from the two thermodynamic cycles (where the uncertainties listed are two standard deviations of the mean) are reported in Table 2. These values are our best determinations of this thermochemistry and used throughout the remainder of the paper along with bond energies for water loss taken from the competitive E_0 results. These values are the ones indicated in Fig. 5. The reliability of the final derived BDEs can be tested by examining the many thermodynamics cycles contained in Fig. 5. One finds that for any cycle (loss of proline from $Na^+Pro(H_2O)_x$ followed by sequential loss of 1–4 water molecules versus sequential loss of these water molecules followed by loss of proline) the deviations are between 0 and 2 kJ/mol, well below the uncertainties involved. In all cases, these comparisons confirm that the BDEs recommended in the present study are self-consistent and compatible with previous work in our lab [24,56].

The experimental results in Table 1 were obtained using molecular parameters for the ground state structures calculated at the B3LYP/6-311 + G** level in all cases (see next section). We checked whether using different molecular structures for the $Na^+Pro(H_2O)_x$ complexes, $x = 1$–4 (especially for $x = 3$ where there are three structures predicted to be the ground state structure by different theoretical methods), changed any of the fitting parameters. In all cases, values for $\sigma_{0,j}$, n, and $E_{0,j}$ were nearly unchanged. The only factors that did change appreciably were entropies of activation, $\Delta S^{\ddagger}$, which characterize the looseness of the transition states involved. Thus, for the $x = 1$ and 2 complexes, the analysis presented in Table 1 uses the ground state isomers identified below, however, for $x = 3$, the data were analyzed using all three possible ground state structures (and their associated vibrational and rotational constants) and the resultant $\Delta S^{\ddagger}$ values listed. For all complexes, the $\Delta S^{\ddagger}$ values for losing water range from −9 to about 40 J/(mol K). The $\Delta S^{\ddagger}$ values for losing proline increase from around 25–30 J/(mol K) for $x = 0$ and 1 to 70–100 J/(mol K) for $x = 2$ and 3. No matter what molecular parameters we use, the entropy of activation for water loss is much smaller, by 30–70 J/(mol K), than for proline loss, which reflects the constraints on the torsional motions of proline when complexed to the sodium ion. For the $x = 3$ complex, two of the possible structures yield small $\Delta S^{\ddagger}$ values for H_2O loss (similar to $x = 1$), implying the structure of the transition state is more similar to the reactant ion than the product (a relatively tight transition state), whereas the third structure gives a much larger $\Delta S^{\ddagger}$ value for losing water that is more similar to $x = 2$ and 4. If the trends are monotonic, which need not be the case, this may indicate that the 3W[bO$^-$,bOH$_2$]-ZW[CO]-C3u structure is the dominant one experimentally.

3.3. Theoretical results

As described above, 6–10 of the lowest energy structures of $Na^+Pro(H_2O)_x$ were optimized at the B3LYP/6-311 + G** level of theory. Among these, pairs of structures that involve slightly different puckering in the five-member pyrrolidine ring of proline (detailed below) show little energy difference (∼1–5 kJ/mol), such that we only discuss and show the lower

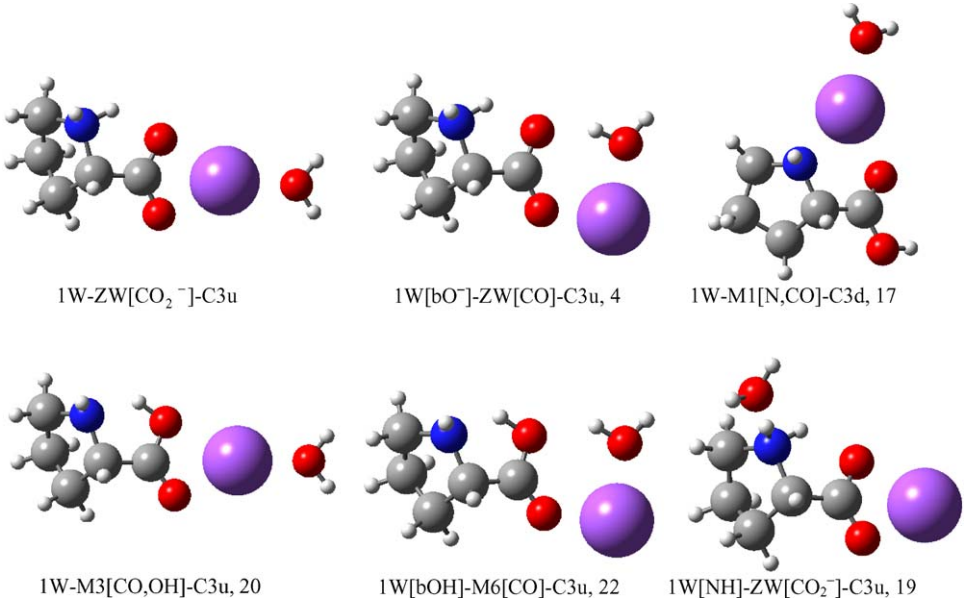

Fig. 6. Optimized structures of $Na^+Pro(H_2O)$ calculated at the B3LYP/6-311 + G** level of theory. Relative energies in kJ/mol from MP2(full)/6-311 + G(2d,2p) single point energy calculations including zero point energies are indicated.

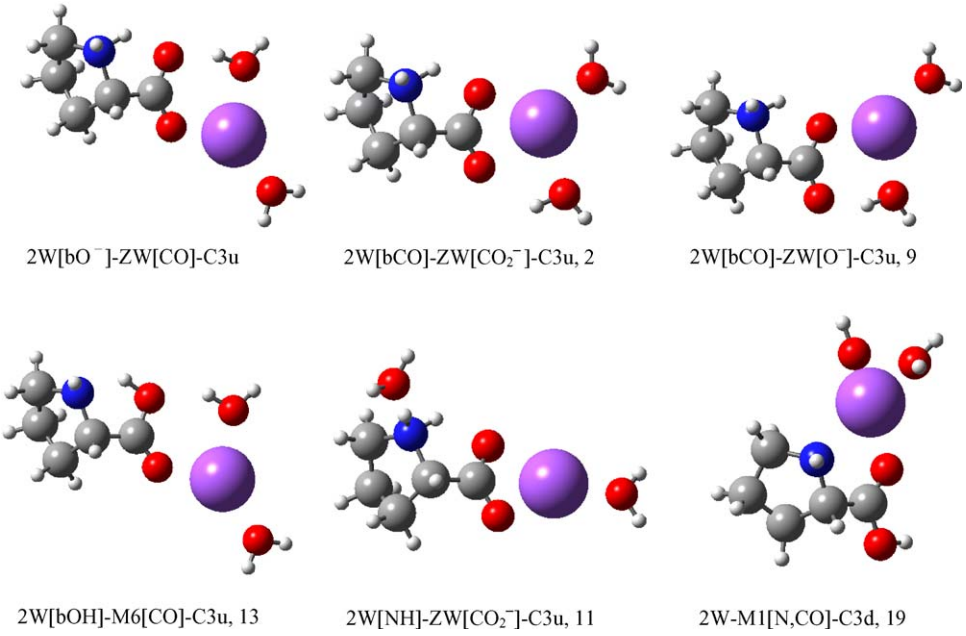

Fig. 7. Optimized structures of $Na^+Pro(H_2O)_2$ calculated at the B3LYP/6-311 + G** level of theory. Relative energies in kJ/mol from MP2(full)/6-311 + G(2d,2p) single point energy calculations including zero point energies are indicated.

energy conformer of each pair. The optimized structures of these lower energy conformers are displayed in Figs. 6–9. The single point energy values including 0 point energy (ZPE) corrections calculated at three different levels of theory relative to the lowest energy isomer are given in Table 3. All relative energies mentioned below are determined at the MP2(full)/6-311 + G(2d,2p)//B3LYP/6-311 + G** level if not otherwise specified.

To identify the structures of the complex, we start with the nomenclature established previously for Na^+Pro [24]. Briefly, for neutral proline, the α carbon is labeled as C1 with the remaining carbon atoms along the ring towards the nitrogen atom labeled as C2–4. All possible puckerings of the five member ring leads to structures in which carbon C3 is out of the plane of the five-member ring [24]. We use a C3u (short for C_3-up) to designate when C3 is cis relative to the COOH or COO^- group. We use C3d (short for C_3-down) to label when these groups are trans to one another. The zwitterion is designated as ZW and nonzwitterionic structures as M*y* (where *y* refers to a specific structure as first designated by Jensen [6]). The notation in brackets after

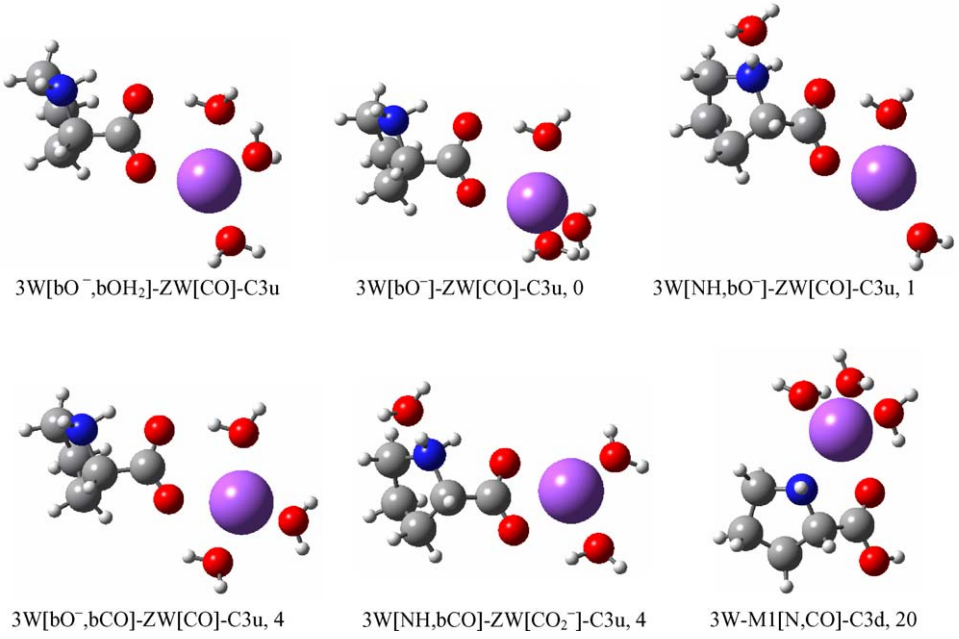

Fig. 8. Optimized structures of $Na^+Pro(H_2O)_3$ calculated at the B3LYP/6-311 + G** level of theory. Relative energies in kJ/mol from MP2(full)/6-311 + G(2d,2p) single point energy calculations including zero point energies are indicated.

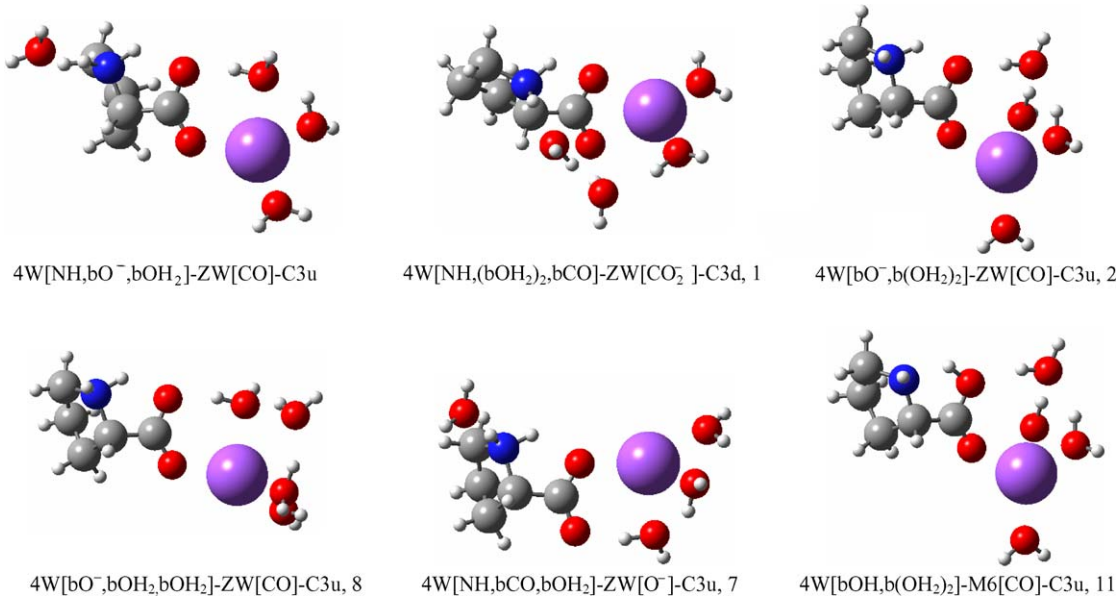

Fig. 9. Optimized structures of $Na^+Pro(H_2O)_4$ calculated at the B3LYP/6-311 + G** level of theory. Relative energies in kJ/mol from MP2(full)/6-311 + G(2d,2p) single point energy calculations including zero point energies are indicated.

these describes the sodium-binding site for each isomer. The *x* W before ZW or M*y* indicates the number of water molecules attached to Na^+Pro, and the notation in brackets after *x* W indicates the water binding site unless the water molecule simply binds to the sodium ion through the oxygen atom. Several important geometric parameters for the $Na^+Pro(H_2O)_x$ complexes are provided in Table 4. For comparison purposes, we optimized the three lowest energy structures of Na^+Pro at the same levels of

Table 3
Relative energy of $Na^+Pro(H_2O)_x$ in kJ/mol[a]

Name	Structure	Theory		
		B3LYP	B3P86	MP2(full)
$Na^+Pro(H_2O)$	1W-ZW[CO_2^-]-C3u	0	0	0
	1W[bO^-]-ZW[CO]-C3u	5.1	2.6	4.2
	1W-M1[N,CO]-C3d	15.9	18.0	17.3
	1W-M3[CO,OH]-C3u	20.2	16.6	19.5
	1W[NH]-ZW[CO_2^-]-C3u	23.1	19.5	19.0
	1W[bOH]-M6[CO]-C3u	23.5	19.2	22.2
$Na^+Pro(H_2O)_2$	2W[bO^-]-ZW[CO]-C3u	0	0	0
	2W[bCO]-ZW[CO_2^-]-C3u	4.6	5.9	2.1
	2W[bCO]-ZW[O^-]-C3u	8.5	9.3	8.8
	2W[bOH]-M6[CO]-C3u	13.3	11.9	13.1
	2W[NH]-ZW[CO_2^-]-C3u	13.7	12.6	11.1
	2W-M1[N,CO]-C3d	21.6	25.2	19.3
$Na^+Pro(H_2O)_3$	3W[NH, bO^-]-ZW[CO]-C3u	0	0	0.8
	3W[bO^-]-ZW[CO]-C3u	0	3.0	0.1
	3W[bO^-,bOH_2]-ZW[CO]-C3u	0.4	2.1	0
	3W[bO^-,bCO]-ZW[CO]-C3u	0.4	2.8	4.4
	3W[NH,bCO]-ZW[CO_2^-]-C3u	7.6	7.7	4.4
	3W[bOH]-M6[CO]-C3u	8.0	10.3	8.3
	3W-M1[N,CO]-C3d	25.1	31.4	19.6
$Na^+Pro(H_2O)_4$	4W[NH,bO^-,bOH_2]-ZW[CO]-C3u	0	0	0
	4W[bO^-,$b(OH_2)_2$]-ZW[CO]-C3u	2.7	3.5	1.9
	4W[NH,$(bOH_2)_2$,bCO]-ZW[CO_2^-]-C3d	6.4	5.4	1.0
	4W[NH,bCO,bOH_2]-ZW[O^-]-C3u	7.2	5.9	6.5
	4W[bO^-,bOH_2,bOH_2]-ZW[CO]-C3u	8.5	5.7	7.6
	4W[bOH,$b(OH_2)_2$]-M6[CO]-C3u	12.5	13.1	11.0

[a] Structures optimized at the B3LYP/6-311 + G** level and all single point energies are calculated using the 6-311 + G(2d,2p) basis set and the indicated level of theory. Zero point energies are included in all values.

Table 4
Geometric parameters of $Na^+Pro(H_2O)_x$ structures optimized at B3LYP/6-311 + G**

Species[a]	$r(Na^+–OC)$ (Å)	$r(Na^+–OH_2)$ (Å)	∠Na^+OC (°)	∠Na^+OCC (°)	∠NCCO (°)	∠CONa^+(OH_2) dihedral (°)
ZW[CO_2^-]-C3u	**2.276**	–	**89.2**	**177.7**	**178.4**	–
M3[CO,OH]-C3u	2.279	–	97.1	178.5	179.1	–
M1[N,CO]-C3d	2.225, 2.427[b]	–	118.5	7.0	3.3	–
1W-ZW[CO_2^-]-C3u	**2.302**	**2.274**	**89.5**	**177.5**	**178.3**	**179.4**
1W[bO$^-$]-ZW[CO]-C3u	2.208	2.203	124.8	176.3	179.6	2.1
1W-M1[N,CO]-C3d	2.253, 2.458[b]	2.272	119.0	8.1	4.1	174.8
1W-M3[CO,OH]-C3u	2.297	2.259	98.8	178.6	179.2	179.2
1W[NH]-ZW[CO_2^-]-C3u	2.265	1.821[c]	89.1	178.2	177.3	–
1W[bOH]-M6[CO]-C3u	2.219	2.226	133.4	177.2	178.7	1.6
2W[bO$^-$]-ZW[CO]-C3u	**2.240**	**2.231**, **2.287**	**126.3**	**176.5**	**179.0**	**2.4, 178.1**
2W[bCO]-ZW[CO_2^-]-C3u	2.489	2.266, 2.291	86.4	177.7	178.3	70.2, 163.3
2W[bCO]-ZW[O$^-$]-C3u	3.276	2.216, 2.289	69.9	177.5	177.1	160.7, 179.1
2W[bOH]-M6[CO]-C3u	2.254	2.253, 2.277	134.9	177.3	178.9	1.1, 179.9
2W[NH]-ZW[CO_2^-]-C3u	2.293	2.277, 1.830[c]	89.3	178.1	177.2	179.0
2W-M1[N,CO]-C3d	2.291, 2.496[b]	2.306, 2.306	119.3	10.6	5.2	106.2, 129.0
3W[NH, bO$^-$]-ZW[CO]-C3u	**2.232**	**2.228**, **2.288**, **1.833**[c]	**125.8**	**177.4**	**178.6**	**1.8, 179.0**
3W[bO$^-$]-ZW[CO]-C3u	2.282	2.273, 2.313, 2.316	127.9	178.8	177.8	1.3, 105.4, 132.2
3W[bO$^-$,bOH_2]-ZW[CO]-C3u	2.266	2.286, 2.299, 2.393	128.1	179.4	178.2	4.6, 63.9, 145.9
3W[bO$^-$,bCO]-ZW[CO]-C3u	2.358	2.260, 2.289, 2.301	126.3	179.5	178.9	5.3, 108.2, 156.2
3W[NH,bCO]-ZW[CO_2^-]-C3u	2.479	2.268, 2.293, 1.831[c]	86.2	178.4	178.0	77.5, 161.7
3W[bOH]-M6[CO]-C3u	2.300	2.290, 2.305, 2.306	136	179.4	179.6	4.8, 102.5, 135.0
3W-M1[N,CO]-C3d	2.391, 2.515[b]	2.309, 2.327, 2.428	119.2	8.6	5.7	88.6, 111.4, 174.2
4W[bNH,bO$^-$,bOH_2]-ZW[CO]-C3u	**2.257**	**2.288**, **2.301**, **2.396**, **1.834**[c]	**127.7**	**178.1**	**178.0**	**4.4, 63.7, 145.1**
4W[bO$^-$,b(OH_2)$_2$]-ZW[CO]-C3u	2.267	2.294, 2.300, 2.315, 3.447[d]	140.2	178.3	178.2	1.1, 48.9, 45.3, 177.9
4W[bNH,(bOH_2)$_2$,bCO]-ZW[CO_2^-]-C3d	2.402	2.286, 2.297, 3.857, 1.820[c]	88.0	172.4	145.7	107.1, 112.2
4W[bNH,bCO,bOH_2]-ZW[O$^-$]-C3u	3.327	2.269, 2.370, 2.408, 1.836[c]	69.0	176.7	177.1	130.6, 167.5, 174.3
4W[bO$^-$,bOH_2,bOH_2]-ZW[CO]-C3u	2.267	2.405, 2.362, 2.277, 3.557[d]	128.5	173.1	179.0	5.2, 42.7, 96.8, 144.6
4W[bOH,b(OH_2)$_2$]-M6[CO]-C3u	2.297	2.288, 2.290, 2.306, 3.562[d]	148.0	179.3	179.7	0.8, 45.8, 47.7, 178.0

[a] Values in bold indicate the lowest energy structures.
[b] The Na^+–N distance.
[c] The NH–OH_2 distance.
[d] Second solvent shell bridging water.

theory used here, B3LYP/6-311 + G**, and include these results in Table 4 as well. These structures and their relative energies are comparable to those elucidated previously at the B3LYP/6-31G* level [24].

3.4. Na^+Pro and $Na^+Pro(H_2O)$

As reported elsewhere for Na^+Pro [11,12,15,24,25], Na^+ favors CO_2^- coordination to zwitterionic proline in the gas phase. The current calculations yield the same results, with ZW[CO_2^-]-C3u being the ground state structure, 21–29 kJ/mol lower than its corresponding nonzwitterion form, M3[CO,OH]-C3u. This is driven by the fact that the secondary amine is more basic than the primary amine available in glycine and all other aliphatic amino acids. The transition state (TS) between ZW[CO_2^-]-C3u and its nonzwitterionic counterpart, M3[CO,OH]-C3u was localized using the synchronous transit-guided quasi-Newton (STQN) method of Schlegel and coworkers [58] at the B3LYP/6-311 + G** level [24]. Single point energies (including ZPE correction) from all three methods listed above using the 6–311 + G(2d,2p) basis set place the TS 15–22 kJ/mol higher in energy relative to ZW[CO_2^-]-C3u and 5–8 kJ/mol lower in energy relative to M3[CO,OH]-C3u. Thus, there is no barrier to the hydrogen transfer once zero point energies are included.

M1[N,CO]-C3d is a nonzwitterion where Na^+ binds in a bidentate configuration to the amino nitrogen and carbonyl oxygen atoms and is aligned approximately with the molecular dipole of proline. It is 19–21 kJ/mol higher than the zwitterion ground state and 2–8 kJ/mol more stable than the M3 structure. Note that for Na^+Gly, the corresponding [N,CO] coordination structure is the global minimum on potential energy surface [4]. We find that the proline backbone molecular structure of M1[N,CO]-C3d is more planar than in Na^+Gly (the ∠NCCO dihedral angles are 3.3° for Na^+Pro and 14.5° for Na^+Gly, respectively) [24]. This implies that the energy of the M1 structure for proline is elevated because of the energetic cost of maintaining the hydrogen atoms on the amine and carbon in an eclipsed conformation and of the constraints imposed on the amino acid backbone by the five-member ring [24].

For $Na^+Pro(H_2O)$, all levels of theory (Table 3) predict the same ground zwitterionic isomer in which the water molecule attaches directly to Na^+ in the Na^+Pro ground isomer to form 1W-ZW[CO_2^-]-C3u, such that the metal ion is three coordinate,

Fig. 6. In both 1W-ZW[CO_2^-]-C3u and the ground zwitterion of Na^+Pro, Na^+ binds in a bidentate configuration to the carboxylic oxygen atoms (CO_2^- coordination) and is approximately aligned with the axis of the molecular dipole of proline. The Na^+–OC distance for Na^+Pro(H_2O) is elongated by 0.026 Å compared to that of Na^+Pro, whereas the ∠Na^+OC bond angle and ∠Na^+OCC and ∠NCCO dihedral angles stay about the same (Table 4). Clearly electron delocalization from the water molecule to Na^+ weakens the binding to proline, but the addition of a water molecule does not change the Na^+Pro structure significantly.

1W[bO^-]-ZW[CO]-C3u is a low-lying zwitterion isomer where the water molecule attaches directly to Na^+ while bridging to the hydroxyl oxygen, forming a pseudo-six member ring, which allows Na^+ to have better alignment with the C=O dipole, the most favorable functional group for binding [4]. (Here and in the following discussion, we use the terms "hydroxyl oxygen" to indicate the oxygen in the CO_2^- group that is in position to accept a proton from the amine and "carbonyl oxygen" to indicate the other oxygen, even though the oxygens no longer retain their identity from the CO_2H moiety.) Thus, this structure lies only 3–5 kJ/mol higher than the ground isomer. The M3 and M6 nonzwitterions, 1W-M3[CO,OH]-C3u and 1W[bOH]-M6[CO]-C3u, are 17–20 kJ/mol above their corresponding zwitterions (5–7 kJ/mol relatively more stable than for Na^+Pro). The increased relative stability of these species is mainly because electron delocalization from water to Na^+ reduces the electrostatic interaction with proline, allowing the proton to return to the oxygen more easily. This is further verified by finding that the transition states between the M3 and M6 isomers and their zwitterion counterparts are 10–16 and 9–17 kJ/mol, respectively, above the zwitterions. This is 5–6 kJ/mol less than for the Na^+Pro ground isomer. Again the proton transfer is barrierless once ZPEs are included, such that M3 and M6 are not actually stable minima.

If the water molecule solvates the positively charged NH_2^+ group instead of binding directly to sodium, the 1W[NH]-ZW[CO_2^-]-C3u structure is formed and lies 19–23 kJ/mol above the ground isomer. The electron delocalization of water on –NH_2^+ reduces the strength of the intramolecular hydrogen bond and strengthens the Na^+–CO_2^- interaction. As a result, the Na^+–OC distance is only 2.265 Å, which is shorter than that of the ground isomer (2.302 Å), and the O···H bond is 1.860 Å versus 1.777 Å in the ground state. The corresponding nonzwitterion of 1W[NH]-ZW[CO_2^-]-C3u is structurally unstable when optimized at the B3LYP/6-311 + G^{**} level and collapses to its zwitterionic form. This is because electron delocalization from the water molecule to the protonated amino nitrogen leads to an even larger basicity of the secondary amine group.

The final low energy structure identified is 1W-M1[N,CO]-C3d, a nonzwitterionic structure where the water molecule binds directly to the sodium ion in the M1[N,CO]-C3d isomer of Na^+Pro, Fig. 6. The M1 structure changes little upon addition of the water (Table 4). This species is located 16–18 kJ/mol higher than the zwitterionic ground isomer. For Na^+Gly(H_2O), this M1 isomer is the lowest energy structure [23].

3.5. $Na^+Pro(H_2O)_2$

Three different levels of theory predict the same ground isomer, 2W[bO^-]-ZW[CO]-C3u, Fig. 7, which can be regarded as the further hydration of the sodium ion in 1W[bO^-]-ZW[CO]-C3u. Further hydration of the sodium ion in the ground isomer of Na^+Pro(H_2O), 1W-ZW[CO_2^-]-C3u, leads to 2W[bCO]-ZW[CO_2^-]-C3u, which lies 2–6 kJ/mol higher in energy. Presumably, these isomers interchange order because of the larger ligand–ligand repulsion (∠H_2O–Na^+–OH_2 of 115° versus 134°). The ∠Na^+OCC and ∠NCCO dihedral angles of these two isomers are close to those of the comparable isomers of Na^+Pro(H_2O); however, the Na^+–OC distances are elongated by 0.032 and 0.187 Å, respectively, and the average Na^+–OH_2 bond distances increase (by 0.056 and 0.005 Å, respectively, Table 4) because of enhanced electron delocalization from water to Na^+. The nonzwitterionic counterpart of the ground isomer is 2W-M6[CO]-C3u, which lies 12–13 kJ/mol higher in energy, compared to 17–20 kJ/mol for Na^+Pro(H_2O) and 21–29 kJ/mol for Na^+Pro. The transition state between them lies 6–12 kJ/mol above 2W[bO^-]-ZW[CO]-C3u and 2–7 kJ/mol below 2W-M6[CO]-C3u when ZPE corrections are included. Again these numbers indicate that transport of the hydrogen atom from the hydroxyl oxygen to the amino nitrogen has no barrier in this configuration.

Another low-lying zwitterion structure is 2W[bCO]-ZW[O^-]-C3u, where the Na^+ now binds to the hydroxyl oxygen atom in the CO_2^- group (the one with the intramolecular hydrogen bond to –NH_2^+) and one water molecule bridges to the carbonyl oxygen atom. Because the bridging water interacts with the carbonyl oxygen, the O···H bridging distance of this structure is 0.021 Å shorter than that of 2W[bO^-]-ZW[CO]-C3u. However, because the Na^+ and –NH_2^+ groups share the electron density of one oxygen atom, this structure lies about ∼9 kJ/mol above the ground structure.

2W[NH]-ZW[CO_2^-]-C3u is a zwitterionic isomer that can be regarded as further hydration of the Na^+ in 1W[NH]-ZW[CO_2^-]-C3u. The Na^+–OC and NH–OH_2 distances are elongated by 0.028 and 0.009 Å, respectively when compared to 1W[NH]-ZW[CO_2^-]-C3u, because of the additional electron delocalization from the water molecule to the charge centers. However, the energy difference (11–14 kJ/mol) relative to the ground isomer is smaller than that for Na^+Pro(H_2O) (19–23 kJ/mol), consistent with better solvation of the Na^+ charge center. The final structure depicted in Fig. 7 is 2W-M1[N,CO]-C3d, which is included for comparison purposes even though it is not among the lowest six energy structures. This M1 isomer maintains a [N,CO] coordination but lies higher in energy (19–25 kJ/mol) compared to analogous structures for Na^+Pro and Na^+Pro(H_2O).

3.6. $Na^+Pro(H_2O)_3$

3W[bO^-,bOH_2]-ZW[CO]-C3u and 3W[bO^-]-ZW[CO]-C3u, zwitterions where the Na^+ is hydrated by three water molecules, are predicted to be the ground structures of Na^+Pro(H_2O)$_3$ by MP2(full) and B3LYP, respectively (Table 3

and Fig. 8). Four coordination of Na^+ is present in both structures with the Na^+ located in a more tetrahedral-like environment in 3W[bO^-]-ZW[CO]-C3u, an environment disrupted by a hydrogen bond between water molecules in 3W[bO^-,bOH_2]-ZW[CO]-C3u. Their proline backbone structures are nearly the same (evident by their similar values for ∠Na^+OC, ∠Na^+OCC, and ∠NCCO, Table 4), except 3W[bO^-,bOH_2]-ZW[CO]-C3u has a Na^+–OC distance shorter by 0.016 Å and 3W[bO^-]-ZW[CO]-C3u has an average Na^+–OH_2 distance longer by 0.023 Å. The Na^+–OC distance in $Na^+Pro(H_2O)_x$ increases from 2.240 Å for $x=2$–2.266 or 2.282 Å for $x=3$ and the average Na^+–H_2O bond distance increases from 2.059 Å to 2.301 or 2.326 Å, consistent with weakening bonds.

A similar structure to these is 3W[bO^-,bCO]-ZW[CO]-C3u, where the Na^+ is also hydrated by three water molecules but now one of them bridges to the carbonyl oxygen atom (O···H bond length = 2.163 Å). The Na^+–OC distance is 0.092 Å longer and the average Na^+–OH_2 distance is 0.043 Å shorter than those of 3W[bO^-,bOH_2]-ZW[CO]-C3u. As might be expected for the subtle geometric changes, this structure lies very low in energy (0–4 kJ/mol higher than the ground isomer, Table 3). Investigations at the B3LYP/6-311 + G^{**} level of the nonzwitterionic forms of these three isomers find that only one is stable, 3W[bOH]-M6[CO]-C3u (not shown in Fig. 8). This M6 structure lies only 8–10 kJ/mol higher than its 3W[bO^-]-ZW[CO]-C3u zwitterionic counterpart, a smaller difference than for $x=0$–2 (25–27, 17–20, 12–13 kJ/mol, respectively) because less electron density is delocalized from the carboxylic group to Na^+ as the number of water molecules increases. The transition state between this zwitterion/charge solvated ion pair is found to be 3–8 kJ/mol higher than the zwitterion and 0–5 kJ/mol lower than the nonzwitterion counterpart when ZPE corrections are included.

3W[NH,bO^-]-ZW[CO]-C3u is predicted to be the lowest energy isomer by both B3LYP and B3P86 methods and its excitation energy is only 0.8 kJ/mol at the MP2(full) level. This zwitterion can be regarded as the addition of the third water molecule to the N-terminus of 2W[bO^-]-ZW[CO]-C3u. This addition decreases the Na^+–OC distance from 2.240 to 2.232 Å, because solvation of the –NH_2^+ center strengthens the Na^+–CO_2^- interaction. The average Na^+–OH_2 bond distance and ∠Na^+OC, ∠Na^+OCC, and ∠NCCO angles (Table 4) stay nearly unchanged. In addition, when comparing the three ground isomers predicted by the different theoretical methods, we find that the proline backbone structures are similar, as indicated by these angles. Note that addition of the water molecule to the –NH_2^+ and Na^+ positions of 2W[bO^-]-ZW[CO]-C3u is essentially isoenergetic (0–2 kJ/mol difference). This observation is the first suggestion that a fourth water molecule may complete the first solvation shell in the Na^+Pro complex.

Further hydration of the sodium ion in 2W[bCO]-ZW[CO_2^-]-C3u, leads to 3W[NH,bCO]-ZW[CO_2^-]-C3u, which lies 4–8 kJ/mol above the ground isomer (2–3 kJ/mol larger than the analogous difference for $x=2$). When compared to 2W[bCO]-ZW[CO_2^-]-C3u, the Na^+–OC distance decreases by 0.01 Å and the average Na^+–OH_2 bond distance and ∠Na^+OC, ∠Na^+OCC, and ∠NCCO angles stay nearly unchanged (Table 4). Such small changes in the proline backbone indicate that the two positively charged sites are largely independent of one another.

The [N,CO] structure, 3W-M1[N,CO]-C3d, lies 20–31 kJ/mol above the ground structure because of the steric crowding around the five-coordinate Na^+. The Na^+–OC distance is elongated by 0.100 Å in the M1 structures of $x=3$ versus 2. The increasing energy difference of this [N,CO] configuration structure relative to the ground isomer from $x=0$ to 3 indicates that further solvation of Na^+ in the nonzwitterionic [N,CO] configuration destabilizes it compared to the ground zwitterionic structure.

3.7. $Na^+Pro(H_2O)_4$

All three levels of theory predict the same ground state structure (Table 3 and Fig. 9), 4W[NH,bO^-,bOH_2]-ZW[CO]-C3u. This geometry can be viewed as attachment of the fourth water to –NH_2^+ of 3W[bO^-,bOH_2]-ZW[CO]-C3u or to Na^+ of 3W[NH,bO^-]-ZW[CO]-C3u. When comparing the structural parameters to those of 3W[NH,bO^-]-ZW[CO]-C3u, we find that the Na^+–OC and the average Na^+–OH_2 bond distances increase from 2.232 and 2.258 Å for $x=3$ to 2.257 and 2.328 Å for $x=4$, respectively, while the NH–OH_2 hydrogen bond distance is almost unchanged. Compared to 3W[bO^-,bOH_2]-ZW[CO]-C3u, the Na^+–OC distance decreases slightly (from 2.266 Å for $x=3$–2.257 Å for $x=4$), while the average Na^+–OH_2 bond distance remains nearly unchanged. Overall, these changes indicate that the NH_2^+ and Na^+ charge sites are relatively decoupled at this level of solvation.

Another low-lying zwitterion in which both positive charge centers are solvated is 4W[NH,bCO,bOH_2]-ZW[O^-]-C3u, which lies 6–7 kJ/mol higher than the ground structure. Here, the Na^+ attaches to the hydroxyl oxygen and uses a water bridge back to the CO group, and the three water molecules attached to Na^+ form two hydrogen bonds to one another. As found for 2W[bCO]-ZW[O^-]-C3u, this structure is energetically less favorable than binding Na^+ to the carbonyl oxygen of the CO_2^- group.

In the remaining low energy structures of $Na^+Pro(H_2O)_4$, the additional water molecule binds in the second solvent shell around the sodium ion. 4W[bO^-,$b(OH_2)_2$]-ZW[CO]-C3u is a zwitterion where three water molecules solvate the Na^+ which binds to proline at the carbonyl oxygen. The fourth water simultaneously hydrogen bonds to two of these water molecules using its two lone pairs of electrons and then bridges to the hydroxyl oxygen atom. The Na^+–O distance of this structure is nearly unchanged when compared to that of 3W[bO^-,bOH_2]-ZW[CO]-C3u, but the ∠Na^+OC bond angle is more linear, 140° versus 128°. This isomer lies only 2–4 kJ/mol above the ground state isomer. The energy difference between this structure and its corresponding nonzwitterionic structure, 4W[bOH,$b(OH_2)_2$]-M6[CO]-C3u, is 9–10 kJ/mol, nearly the same as that for the analogous $x=3$ complexes. The transition state between this zwitterion/charge solvated pair was not located at the present level of theory, probably because of the very floppy motions associated with four water molecules. On the basis of the

smaller complexes, it seems likely that the proton transfer to form the zwitterion is barrierless once ZPE corrections are included. Another structure that exhibits hydrogen bonds between water molecules solvating the Na^+ charge center is 4W[bO$^-$,bOH$_2$,bOH$_2$]-ZW[CO]-C3u, which can be formed by moving the water from the NH position in the ground 4W[NH,bO$^-$,bOH$_2$]-ZW[CO]-C3u isomer to Na^+. Here the additional water molecule is in the second solvent shell but hydrogen bonds using one of its covalently bound hydrogens. This species lies 6–9 kJ/mol higher in energy, showing that solvation of the NH_2^+ charge center is now more favorable than additional solvation of Na^+.

Perhaps the most surprising low energy isomer is 4W[NH,(bOH$_2$)$_2$,bCO]-ZW[CO$_2^-$]-C3d, which is only 1–6 kJ/mol higher than the ground isomer. This structure can be viewed as starting with 2W[bCO]-ZW[CO$_2^-$]-C3d, solvating the NH_2^+ center, and then using the last water in a second solvent shell to hydrogen bond simultaneously to the water on NH_2^+, a water on Na^+, and the carbonyl oxygen. This leads to pseudo six and seven-membered rings and causes the C_α–CO single bond of proline to rotate ∼32° relative to the ground structure (as evidenced by the change of ∠NCCO from about 178° to 146°, Table 4). Note that the NH–OH$_2$ bond distance is 0.014 Å shorter while the NH–O bond distance is 0.168 Å longer in this structure compared to that of the ground isomer. This indicates that more electron density is delocalized onto –NH_2^+ through the second bridging water molecule, leading to a stronger electrostatic interaction between the bridging water and –NH_2^+ charge center and a weaker intramolecular hydrogen bond.

4. Discussion

4.1. Trends in experimental bond dissociation energies

Our best results for the energies required to remove water and proline from $Na^+Pro(H_2O)_x$, $x = 1$–4, are shown in Fig. 5 (competitive analysis thresholds for losing water, Table 1, and the weighted average for losing proline from Table 2) along with previous experimental results for both $D_0(Na^+$–Pro) [24] and the hydration energies of Na^+ [56]. Similar to the $Na^+(H_2O)_x$ system, the BDEs of water to sodiated proline decrease (from 66 ± 5 to 20 ± 6 kJ/mol) with increasing number of water molecules because of increasing steric effects and decreasing effective charge on the sodium ion. The first and second water BDEs to sodiated proline (66 ± 5 and 45 ± 5 kJ/mol) are comparable to those of the third and fourth water to sodium ion (70 ± 6 and 55 ± 8 kJ/mol) in the $Na^+(H_2O)_x$ system [56]. This correspondence implies that the solvation effect of proline on a sodium ion is slightly larger than that of two water molecules. Indeed, the BDE of proline to sodium ion is 186 ± 4 kJ/mol [24], slightly larger than the sum of the BDEs for the first and second water on Na^+ (177 ± 10 kJ/mol) [56]. In addition, experimental BDEs of proline to $Na^+(H_2O)_x$ also decrease (from 186 ± 4 to 46 ± 17 kJ/mol) with increasing solvation from $x = 0$ to 4. Clearly, the experimental BDEs for losing water or proline decrease monotonically with increasing number of water molecules. The BDE for losing proline is larger than that for losing water from each $Na^+Pro(H_2O)_x$ complex, $x = 1$–4, consistent with the qualitative dissociation behavior exhibited in Figs. 1–4.

The experimental binding energy of the fourth water molecule is measured to be 20 ± 6 kJ/mol, nearly equal to the energy associated with the hydrogen bonding network in pure water, 23 kJ/mol [59]. This result implies that the fourth water is either hydrogen bonding to proline or other water molecules that belong to the first solvent shell of Na^+. Indeed, all levels of theory predict the same zwitterionic ground isomer of $Na^+Pro(H_2O)_4$, 4W[NH,bO$^-$,bOH$_2$]-ZW[CO]-C3u, Fig. 9, where one of the water molecules hydrogen bonds to –NH_2^+ and Na^+ is tetracoordinate with its first solvent shell formed by the carbonyl oxygen and the other three water molecules. One imagines that any additional water molecules will hydrogen bond primarily to the water molecules already present, leading to BDEs that are comparable to that of the fourth water ligand bond, while continuing to favor the zwitterionic form of proline.

4.2. Conversion from 0 to 298 K

Conversion from 0 K bond energies to 298 K bond enthalpies and free energies is accomplished using the rigid rotor/harmonic oscillator approximation and the frequencies calculated at the B3LYP/6-311 + G** level. These ΔH_{298} and ΔG_{298} values along with the conversion factors and the 0 K enthalpies are reported in Table 5. The uncertainties listed are determined by scaling most of the vibrational frequencies by ±10% along with twofold variations in the metal–ligand frequencies.

Our calculations of $\Delta H_{298} - \Delta H_0$ and $T\Delta S_{298}$ show little difference (∼1 kJ/mol) between the C3-up and C3-down conformer pairs, such that the resulting difference in the ΔG_{298} values remain similar to the ΔH_0 values. Calculating the equilibrium population at room temperature, the ground C3-up conformer is dominant (70–90% for $x = 1$, 2, and 4, 50–70% for $x = 3$, depending on the level of theory). In order to simplify the discussion below, we will only compare the ΔH_{298} and ΔG_{298} values of the zwitterionic C3-up conformer for each x. In general, the room temperature enthalpies, ΔH_{298}, are nearly the same as the 0 K values, ΔH_0, with a maximum difference of ∼3 kJ/mol in case of $x = 2$. The ΔG_{298} values decrease from 155.4 ± 5.4 to −6.4 ± 14.5 kJ/mol for losing proline and from 37.5 ± 8.7 to −17.0 ± 10.2 kJ/mol for losing water. Note that the ΔG_{298} values for losing water and proline from $Na^+Pro(H_2O)_4$ are negative, which indicates that the equilibrium for generating this ion lies to the smaller $Na^+Pro(H_2O)_3$ complex. This is consistent with the low absolute intensities found for the $Na^+Pro(H_2O)_4$ beams. It is possible that this adversely affects our threshold measurements for the $Na^+Pro(H_2O)_4$ complex although such an effect was not evident in our previous work on $Na^+Gly(H_2O)_4$, which also has a negative free energy of dissociation [23].

We also calculated the ΔG_{298} values for all low-lying structures of $x = 1$–4. For $x = 1$, we find that the calculated ΔG_{298} excitation energies of the second lowest energy structure, 1W[bO$^-$]-ZW[CO]-C3u, are >12 kJ/mol, compared to only 2–5 kJ/mol in the ΔH_0 values (Table 3). This is because the bridging water

Table 5
Enthalpies and free energies of H_2O and proline binding energies (kJ/mol) for $Na^+Pro(H_2O)_x$ at 0 and 298 K[a]

Complex	Ionic product	ΔH_0[a]	$\Delta H_{298} - \Delta H_0$[b]	ΔH_{298}	$T\Delta S_{298}$[b]	ΔG_{298}
Na^+Pro	Na^+	186.0 (4)	1.7 (0.8)	187.7 (4.1)	32.4 (3.5)	155.4 (5.4)
$Na^+Pro(H_2O)$	Na^+Pro	66.3 (5)	−0.2 (1.2)	66.1 (5.1)	28.6 (7.1)	37.5 (8.7)
	$Na^+(H_2O)$	158(15)	−2.1 (1.7)	156 (15)	33.8 (10.0)	122 (18)
$Na^+Pro(H_2O)_2$	$Na^+Pro(H_2O)$	44.5 (5)	2.6 (1.5)	47.1 (5.1)	41.9 (5.4)	5.3 (7.5)
	$Na^+(H_2O)_2$	121(15)	0.3 (1.9)	121 (15)	47.4 (8.3)	74 (17)
$Na^+Pro(H_2O)_3$	$Na^+Pro(H_2O)_2$	30.2 (4)	1.8 (2.5)	32.1 (4.7)	39.3 (7.8)	−7.3 (9.1)[c]
	$Na^+(H_2O)_3$	82(10)	1.5 (2.1)	82.5 (10)	54.9 (8.1)	27.6 (13)[c]
$Na^+Pro(H_2O)_4$	$Na^+Pro(H_2O)_3$	20.3 (6)	1.8 (2.5)	22.1 (6.5)	39.2 (7.8)	−17.0 (10.2)
	$Na^+(H_2O)_4$	46(17)	1.5 (2.4)	48.5 (17)	54.9 (9.3)	−6.4 (17)

[a] Experimental values from this work (Table 1).
[b] Values were computed using standard formulas and molecular constants calculated at the B3LYP/6-311 + G** level. The uncertainties correspond to 10% variations in the vibrational frequencies of the ligands and two-fold variations in the metal–ligand-frequencies.
[c] Values using 3W[bO^-,bOH_2]-ZW[CO]-C3u structure parameters. $T\Delta S_{298}$ and ΔG_{298} values for 3W[bNH, bO^-]-ZW[CO]-C3u and 3W[bO^-]-ZW[CO]-C3u are 32.1 (8.3) and 30.6 (10.6), −2.8 (9.1) and −0.8 (11.7) for losing water, 47.6 (8.5) and 46.1 (10.9), 32.1 (12) and 34.1 (15) for losing proline, respectively.

gives a larger $T\Delta S_{298}$ value for 1W[bO^-]-ZW[CO]-C3u. This large ΔG_{298} difference means that the population of the second lowest isomer is calculated to be <1% in the flow tube at room temperature. For $x = 2$, the ΔG_{298} excitation energies of the second lowest energy structure, 2W[bCO]-ZW[CO_2^-]-C3u, are −1 (MP2) or 3 (B3P86) kJ/mol, compared to 2–6 kJ/mol for ΔH_0 (Table 3). Thus, this "excited" isomer comprises 20–60% of the $x = 2$ complexes found in our flow tube system with the ground isomer making up the remainder. If the data are reanalyzed using molecular parameters of both low energy structures, the ΔH_0 shifts lower by ∼1 kJ/mol than the value reported in Table 5. Among the five low-lying structures for $x = 3$ (Table 3), we find that the ΔH_{298} and ΔG_{298} values for losing water and proline remain close to each other except for 3W[bO^-,bOH_2]-ZW[CO]-C3u, which lies relatively high in free energy (6–8 kJ/mol). The small energy differences among the remaining four isomers indicate that there is likely to be a mixture of these low-lying structures in our flow tube. Reanalysis of the data for losing water and proline using the parameters of these low energy structures show almost identical results as those reported in Table 5, which use the structural parameters of 3W[NH, bO^-]-ZW[CO]-C3u. For $x = 4$, calculations show that the ground structure, 4W[bNH,bO^-,bOH_2]-ZW[CO]-C3u, is dominant (over 90% in population) at room temperature.

4.3. Comparison of theoretical and experimental bond dissociation energies

In addition to our calculations of the $Na^+Pro(H_2O)_x$ complexes, we also performed parallel calculations for $Na^+(H_2O)_x$, $x = 1$–4, using the B3LYP/6-311 + G** level of theory for the geometries and single point energy calculations using B3LYP, B3P86, and MP2(full) levels with the 6-311 + G(2d,2p) basis set, including ZPE and BSSE corrections. This yields BDEs (in kJ/mol) at these three levels of theory of 94.3, 91.0, and 88.9 for $x = 1$; 82.8, 79.9, and 78.6 for $x = 2$; 65.0, 63.0, and 63.5 for

Table 6
H_2O and proline binding energies (kJ/mol) for $Na^+Pro(H_2O)_x$ at 0 K[a]

Complex	Ionic product	Experiment	B3LYP	B3P86	MP2(full)
Na^+ Pro	Na^+	186 (4)[b]	196.1	188.3	184.1
$Na^+Pro(H_2O)$	Na^+Pro	66 (5)[c]	66.6	64.4	63.4
	$Na^+(H_2O)$	158 (15)[d]	167.6	162.8	159.2
$Na^+Pro(H_2O)_2$	$Na^+Pro(H_2O)$	45 (5)[c]	54.5	54.5	54.2
	$Na^+(H_2O)_2$	121 (15)[d]	138.7	136.5	132.7
$Na^+Pro(H_2O)_3$	$Na^+Pro(H_2O)_2$	30 (4)[c]	40.9	42.1	41.8
	$Na^+(H_2O)_3$	82 (10)[d]	113.1	113.8	106.1
$Na^+Pro(H_2O)_4$	$Na^+Pro(H_2O)_3$	20 (6)	38.9	38.7	38.1
	$Na^+(H_2O)_4$	46 (17)[d]	99.2	103.1	94.8
MAD[e]	$-H_2O$		10 (8)	10 (7)	10 (6)
	–Pro		24 (18)	22 (23)	18 (20)

[a] Energies calculated at the corresponding 6-311 + G(2d,2p)//B3LYP/6-311 + G** level. Zero point energies and BSSE corrections are included for all.
[b] From Moision and Armentrout [24].
[c] From competitive fitting.
[d] Weighted average values.
[e] Mean absolute deviation from the experimental values.

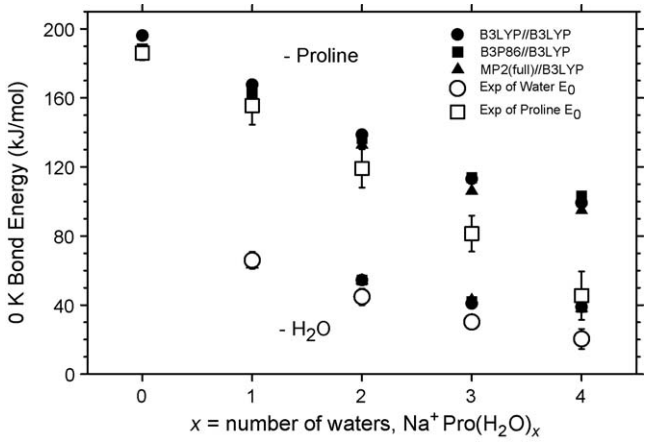

Fig. 10. Comparison of experimental (open symbols) and theoretical (closed symbols) 0 K BDE values in kJ/mol for loss of proline (upper values) and water (lower values) from $Na^+Pro(H_2O)_x$ as a function of x.

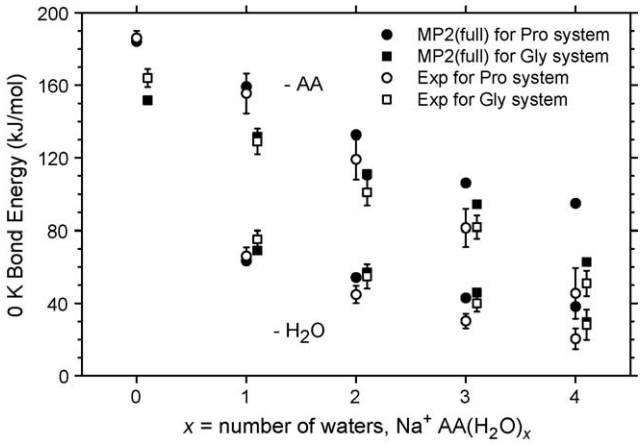

Fig. 11. Comparison of experimental (open symbols) and MP2 (closed symbols) values for loss of the amino acid (AA, upper values) and water (lower values) from $Na^+Gly(H_2O)_x$ and $Na^+Pro(H_2O)_x$ as a function of x.

$x = 3$; and 53.0, 50.3, and 53.3 for $x = 4$. Almost all the calculated values are within the experimental uncertainties [56], with mean absolute deviations (MADs) of 2 ± 2, 4 ± 2, and 4 ± 2 kJ/mol, respectively, at the three levels of theory (B3LYP, B3P86, and MP2).

The theoretical BDEs for the $Na^+Pro(H_2O)_x$ complexes calculated at three levels of theory are compared to the experimental values in Table 6. We find that all three theoretical methods (B3LYP, B3P86, and MP2) yield BDE values of $Na^+Pro(H_2O)_x$ system that differ little from one another and overall show reasonable agreement with our experimental values, Fig. 10, although with notable exceptions. MADs from experiment are 10 ± 8, 10 ± 7, and 10 ± 6 kJ/mol, respectively, for losing water and 24 ± 18, 22 ± 23, and 18 ± 20 kJ/mol, respectively, for losing proline. The MP2(full) results give marginally the best comparison to experiment. In contrast to the $Na^+(H_2O)_x$ results, the theoretical values for loss of water overestimate our experimental results by ~10 kJ/mol for $x = 2$ and 3 and by ~19 kJ/mol for $x = 4$, where the latter discrepancy exceeds any reasonable experimental uncertainty. The calculated BDEs for losing proline from the Na^+Pro [24] and $Na^+Pro(H_2O)$ complexes show good agreement with the experimental values although the B3LYP values are high by about 10 kJ/mol (a result typical for this level of theory [54]). For the $x = 2$–4 complexes, the calculated BDEs for losing proline from $Na^+Pro(H_2O)_x$ are again systematically higher than the experimental values by about 10, 20, and 50 kJ/mol, respectively, well outside the experimental uncertainty in the latter case. Note that the agreement between experiment and theory would degrade even further if the results from single channel or competitive fitting (Table 2) were used as our best experimental results instead of those from the thermodynamic cycles. Overall the agreement between experimental and theoretical BDEs is reasonable, except for the case of $Na^+Pro(H_2O)_4$ where both experiment and theory may be reaching their limits of accuracy.

As depicted in Fig. 10, the BDEs obtained from our experiments and calculations for $Na^+Pro(H_2O)_x$, $x = 0$–3, qualitatively follow the same trends, decreasing monotonically at a somewhat faster rate experimentally than theoretically. However, the calculated BDEs for losing one water and proline from the $Na^+Pro(H_2O)_4$ complex are just slightly smaller than those for the $Na^+Pro(H_2O)_3$ complex, and therefore are much larger than the corresponding experimental BDEs. The monotonic decrease in the BDEs for $Na^+Pro(H_2O)_x$ with increasing x is primarily a result of the increasing ligand–ligand repulsion and increased charge solvation. The more water molecules around Na^+, the more weakly Na^+ interacts with H_2O and proline.

4.4. Comparison of two systems: $Na^+Pro(H_2O)_x$ and $Na^+Gly(H_2O)_x$

The experimental and MP2(full) theoretical BDEs of hydrated Na^+Gly and Na^+Pro complexes are compared in Fig. 11. Similar to the $Na^+Gly(H_2O)_x$ system [4,23,56], the BDEs for losing proline from $Na^+Pro(H_2O)_x$ are much higher than the BDEs for losing water at each x, where $x = 0$–4 [24,56]. BDEs for losing water from $Na^+Pro(H_2O)_x$ are 9–12 kJ/mol lower than the corresponding BDEs for $Na^+Gly(H_2O)_x$ system at all x, $x = 1$–4. This is consistent with proline being a better ligand than glycine, as reflected by the experimental BDE of Na^+ to proline being 22 kJ/mol larger than that to glycine [4,24]. Theory finds a similar trend for $x = 1$–3, although with smaller differences of 3–11 kJ/mol, except for $x = 4$, where the fourth water binds more tightly in the proline system by 8–9 kJ/mol.

For proline, Na^+ chelates to the CO_2^- group of zwitterionic proline, whereas Na^+ binds to glycine in a [N,CO] configuration. Calculations find that the BDE of proline to Na^+ is 26–30 kJ/mol larger than that of glycine, a difference that is comparable to the calculated excitation energy of the [N,CO] isomer of Na^+Pro, 19–21 kJ/mol [12,24]. Thus, the [N,CO] configurations have similar absolute BDEs for both proline and glycine, suggesting that the enhanced binding of proline versus glycine can be attributed to the charge separation inherent in the zwitterion. As water molecules are added to these complexes,

we find that the experimental BDEs of the amino acid to $Na^+(H_2O)_x$ decrease monotonically with increasing solvation from $x=0$ to 4, Fig. 11. However, the BDEs for the proline system decline more rapidly such that the BDEs are comparable for $x=3$ (81 ± 10 and 82 ± 6 kJ/mol for proline and glycine, respectively) and the BDE for proline is slightly smaller for $x=4$. Theory finds a similar trend for $x=0$–3 except that the proline binding remains stronger throughout. Thus, the faster decrease in the amino acid BDEs for proline versus glycine appears to be the result of solvation decreasing the extent of the charge separation in the zwitterion. This is consistent with the observation that the NH···OC intramolecular hydrogen bond lengths in $Na^+Pro(H_2O)_x$ decrease as x increases, 1.805, 1.777, 1.752, and 1.732 Å for $x=0$–3, respectively, in the structures where only Na^+ is solvated.

Theoretical calculations show that the ground state structures are nonzwitterionic for $Na^+Gly(H_2O)_x$ and zwitterionic for $Na^+Pro(H_2O)_x$, where $x=0$–4. As noted above, Na^+ binds to glycine with a [N,CO] configuration and to proline at the CO_2^- group. The first water binds directly to Na^+ for both amino acids. For $x=2$–4, the most favorable binding sites for Na^+ to both amino acids change to CO coordination with one water molecule bridging to the hydroxyl oxygen. In the glycine system, the ground state isomers for $x=1$–4 have all water molecules solvating Na^+. In the proline system, this is also true for $x=1$ and 2, whereas solvation of the $-NH_2^+$ group leads to isomers at a much higher energies (19–23 and 11–14 kJ/mol for proline, Table 3, versus 34–45 and 24–26 kJ/mol for glycine, respectively). For $x=3$, structures of $Na^+Pro(H_2O)_3$ in which only Na^+ is solvated and both $-NH_2^+$ and Na^+ are solvated are predicted to be comparable in energy, whereas for $Na^+Gly(H_2O)_3$, the structure in which both charge centers are solvated is 8–13 kJ/mol higher in energy than the ground structure where only Na^+ is solvated. For $Na^+Pro(H_2O)_4$, the structure where both $-NH_2^+$ and Na^+ are solvated becomes the most stable configuration for zwitterionic proline, and this completes the first solvent shell for Na^+Pro. In other words, these four water molecules interact electrostatically and directly with zwitterionic Na^+Pro, whereas additional water molecules are likely to preferentially bind to these inner shell water molecules. In the glycine system, zwitterionic isomers in which both charge centers are solvated become favorable at about $x=4$ (0–10 kJ/mol higher than the ground isomer) although we have projected that such structures will not be the clear ground states until the first solvent shell is completed at about five or six water molecules [23]. These comparisons indicate that the more basic secondary amine group of proline and the resultant charge separation of the zwitterionic complex formed induce a smaller first solvent shell (four waters) for Na^+Pro versus that for Na^+Gly (5–6 waters). In part, this is because the cyclic structure of proline allows only an NH_2^+ group in its zwitterionic state, whereas glycine has an NH_3^+ group. In both sodiated complexes, one of the NH bonds is involved in an intramolecular hydrogen bond back to an oxygen on the CO_2^- group, which means that inner shell solvation of the protonated nitrogen center requires only one water molecule for proline compared to two for glycine.

5. Conclusions

The kinetic energy dependences of the collision-induced dissociation (CID) of $Na^+Pro(H_2O)_x$, where $x=1$–4, are examined in a guided ion beam mass spectrometer. The primary process observed in all cases is the loss of water from the complex. Sequential losses of water ligands are also observed for $x=2$–4. The cross-sections for losing proline from the complex are also observed at much higher energies for $x=1$–3 and are about 1 order of magnitude smaller than those for losing water. BDEs at 0 K for losing water from the complexes are measured from the threshold behavior and those for losing proline are derived from thermodynamic cycles. The resulting experimental results show that the sequential binding energies for losing water or proline from $Na^+Pro(H_2O)_x$ decrease monotonically with increasing x. These trends are explained by increasing ligand–ligand repulsion and decreasing effective charge on the sodium ion as water molecules are added to the complex.

Three different levels of ab initio calculations including zero point energy corrections and basis set superposition errors were performed for $Na^+Pro(H_2O)_x$, $x=0$–4. Both experiment and calculations find the same general trends in the BDEs with increasing solvation, Fig. 10. The calculated BDEs for losing water and proline agree reasonably well with our absolute experimental values for $x=0$–3, but fall well outside of our experimental uncertainties for $x=4$. It is unclear whether this is a limitation in the experiments for these weakly bound complexes or in the theory for such a floppy molecule.

In the Na^+Pro complex, theory indicates that the sodium ion prefers to bind in a bidentate configuration to the carboxylic acid oxygen atoms of zwitterionic proline (CO_2^- coordination) [24]. The first water attaches directly to the sodium ion without influencing the proline conformation. However, for $x=2$–4, the Na^+ binding site changes CO coordination with one of the water molecules bridging to the hydroxyl oxygen. For $x=3$, there are four isomers lying sufficiently low in energy that they could be populated in our experiment, which emphasizes that the third water can bind to Na^+ or $-NH_2^+$ with nearly equal facility. For $x=4$, the unique ground structure has a completely solvated tetracoordinate Na^+ and solvated $-NH_2^+$ group. Low-lying structures of this complex all involve additional water molecules binding in the second solvent shell.

When comparing $Na^+Pro(H_2O)_x$, $x=1$–4, to the analogous glycine system [23], we find that the BDEs for losing water from $Na^+Gly(H_2O)_x$ are 9–12 kJ/mol larger than those of $Na^+Pro(H_2O)_x$ at each x. Such correspondence is consistent with the fact that Na^+ binds to zwitterionic proline more strongly than to nonzwitterionic glycine. BDEs for losing glycine are 22 ± 7, 27 ± 13 and 18 ± 13 kJ/mol smaller than those for losing proline for $x=0$–2, respectively, nearly equal to each other for $x=3$, and the glycine BDE is slightly larger for $x=4$. This trend indicates that the charge separated zwitterionic Na^+Pro system is more strongly influenced by solvation than the nonzwitterionic Na^+Gly complex. Indeed, theory finds that all ground state structures for $Na^+Gly(H_2O)_x$, $x=0$–4, are nonzwitterionic (charge solvated) [23], whereas $Na^+Pro(H_2O)_x$ is zwitterionic for $x=0$–4.

Acknowledgments

This work is supported by the National Science Foundation under Grant No. CHE-0451477. A grant of computer time from the Center for High Performance Computing in University of Utah is gratefully acknowledged.

References

[1] C.H. Suelter, Science 168 (1970) 789.
[2] T.M. Larsen, L.T. Laughlin, H.M. Holden, I. Rayment, G.H. Reed, Biochemie 33 (1994) 6301.
[3] C.K. Mathews, K.E. van Holde, Biochemistry, The Benjamin/Cummings Publishing Company, Redwood City, 1990.
[4] R.M. Moision, P.B. Armentrout, J. Phys. Chem. A 106 (2002) 10350.
[5] R.M. Moision, P.B. Armentrout, Phys. Chem. Chem. Phys. 6 (2004) 2588.
[6] F. Jensen, J. Am. Chem. Soc. 114 (1992) 9533.
[7] J.S. Klassen, S.G. Anderson, A.T. Blades, P. Kebarle, J. Phys. Chem. 100 (1996) 14218.
[8] L. Rodriguez-Santiago, M. Sodupe, J. Tortajada, J. Phys. Chem. A 105 (2001) 5340.
[9] B.A. Cerda, C. Wesdemiotis, Analyst 125 (2000) 657.
[10] B.A. Cerda, S. Hoyau, G. Ohanessian, C. Wesdemiotis, J. Am. Chem. Soc. 120 (1998) 2437.
[11] S. Hoyau, K. Norrman, T.B. McMahon, G. Ohanessian, J. Am. Chem. Soc. 121 (1999) 8864.
[12] C. Kapota, J. Lemaire, P. Maitre, G. Ohanessian, J. Am. Chem. Soc. 126 (2004) 1836.
[13] T. Shoeib, A.C. Hopkinson, K.W.M. Siu, J. Phys. Chem. B. 105 (2001) 12399.
[14] T. Shoeib, K.W.M. Siu, A.C. Hopkinson, J. Phys. Chem. A 106 (2002) 6121.
[15] T. Marino, N. Russo, M. Toscano, J. Phys. Chem. B. 107 (2003) 2588.
[16] T. Wyttenbach, M. Witt, M.T. Bowers, J. Am. Chem. Soc. 122 (2000) 3458.
[17] M.T. Rodgers, P.B. Armentrout, Mass Spectrom. Rev. 19 (2000) 215.
[18] M.T. Rodgers, P.B. Armentrout, Acc. Chem. Res. 37 (2004) 989.
[19] R.A. Jockusch, A.S. Lemoff, E.R. Williams, J. Phys. Chem. A 105 (2001) 10929.
[20] R.A. Jockusch, A.S. Lemoff, E.R. Williams, J. Am. Chem. Soc. 123 (2001) 12255.
[21] A.S. Lemoff, M.F. Bush, E.R. Williams, J. Am. Chem. Soc. 125 (2003) 13576.
[22] A.S. Lemoff, E.R. Williams, J. Am. Soc. Mass. Spectrom. 15 (2004) 1014.
[23] S.J. Ye, R.M. Moision, P.B. Armentrout, Int. J. Mass Spectrom. 240 (2005) 233.
[24] R.M. Moision, P.B. Armentrout, J. Phys. Chem. A 110 (2006) 3933.
[25] A.S. Lemoff, M.F. Bush, E.R. Williams, J. Phys. Chem. A 109 (2005) 1903.
[26] K.M. Ervin, P.B. Armentrout, J. Chem. Phys. 80 (1984) 2978.
[27] F. Muntean, P.B. Armentrout, J. Chem. Phys. 115 (2001) 1213.
[28] E.R. Fisher, P.B. Armentrout, J. Chem. Phys. 94 (1991) 1150.
[29] E.R. Fisher, B.L. Kickel, P.B. Armentrout, J. Chem. Phys. 97 (1992) 4859.
[30] R.H. Schultz, K.C. Crellin, P.B. Armentrout, J. Am. Chem. Soc. 113 (1991) 8590.
[31] M.T. Rodgers, P.B. Armentrout, J. Phys. Chem. A 101 (1997) 1238.
[32] K.M. Ervin, P.B. Armentrout, J. Chem. Phys. 83 (1985) 166.
[33] E. Teloy, D. Gerlich, Chem. Phys. 4 (1974) 417.
[34] D. Gerlich, Adv. Chem. Phys. 82 (1992) 1.
[35] N.R. Daly, Rev. Sci. Instrum. 31 (1960) 264.
[36] D.A. Hales, L. Lian, P.B. Armentrout, Int. J. Mass Spectrom. Ion Process. 102 (1990) 269.
[37] T.S. Beyer, D.F. Swinehart, Commun. Assoc. Comput. Mach. 16 (1973) 379.
[38] M.T. Rodgers, P.B. Armentrout, J. Chem. Phys. 109 (1998) 1787.
[39] R.G. Gilbert, S.C. Smith, Theory of Unimolecular and Recombination Reactions, Blackwell Scientific, London, 1990.
[40] M.T. Rodgers, K.M. Ervin, P.B. Armentrout, J. Chem. Phys. 106 (1997) 4499.
[41] E.V. Waage, B.S. Rabinovitch, Chem. Rev. 70 (1970) 377.
[42] P.B. Armentrout, J. Simons, J. Am. Chem. Soc. 114 (1992) 8627.
[43] D.A. Pearlman, D.A. Case, J.W. Caldwell, W.R. Ross, T.E. Cheatham, S. DeBolt, D. Ferguson, G. Seibel, P. Kollman, Comp. Phys. Commun. 91 (1995) 1.
[44] High Performance Computational Chemistry Group, NWChem, A Computational Chemistry Package for Parallel Computers, Pacific Northwest National Laboratory, Richland, Washington 99352, 2003.
[45] C.C.J. Roothan, Rev. Mod. Phys. 23 (1954) 69.
[46] J.S. Binkley, J.A. Pople, W.J. Hehre, J. Am. Chem. Soc. 102 (1951) 939.
[47] M.J. Frisch, G.W. Trucks, H.B. Schlegel, G.E. Scuseria, M.A. Robb, J.R. Cheeseman, J.A. Montgomery, T. Vreven, K.N. Kudin, J.C. Burant, J.M. Millam, S.S. Iyengar, J. Tomasi, V. Barone, B. Mennucci, M. Cossi, G. Scalmani, N. Rega, G.A. Petersson, H. Nakatsuji, M. Hada, M. Ehara, K. Toyota, R. Fukuda, J. Hasegawa, M. Ishida, T. Nakajima, Y. Honda, O. Kitao, H. Nakai, M. Klene, X. Li, J.E. Knox, H.P. Hratchian, J.B. Cross, C. Adamo, J. Jaramillo, R. Gomperts, R.E. Stratmann, O. Yazyev, A.J. Austin, R. Cammi, C. Pomelli, J.W. Ochterski, P.Y. Ayala, K. Morokuma, G.A. Voth, P. Salvador, J.J. Dannenberg, V.G. Zakrzewski, S. Dapprich, A.D. Daniels, M.C. Strain, O. Farkas, D.K. Malick, A.D. Rabuck, K. Raghavachari, J.B. Foresman, J.V. Ortiz, Q. Cui, A.G. Baboul, S. Clifford, J. Cioslowski, B.B. Stefanov, G. Liu, A. Liashenko, P. Piskorz, I. Komaromi, R.L. Martin, D.J. Fox, T. Keith, M.A. Al-Laham, C.Y. Peng, A. Nanayakkara, M. Challacombe, P.M.W. Gill, B. Johnson, W. Chen, M.W. Wong, C. Gonzalez, J.A. Pople, Gaussian 03, Revision B. 02, Gaussian, Inc., Pittsburgh, PA, 2003.
[48] A.D. Becke, J. Chem. Phys. 98 (1993) 5648.
[49] R. Ditchfield, W.J. Hehre, J.A. Pople, J. Chem. Phys. 72 (1971) 5639.
[50] A.D. McLean, G.S. Chandler, J. Chem. Phys. 72 (1980) 5639.
[51] R. Krishnan, J.S. Binkley, R. Seeger, J.A. Pople, J. Chem. Phys. 72 (1980) 650.
[52] J.A. Montgomery Jr., M.J. Frisch, J.W. Ochterski, G.A. Petersson, J. Chem. Phys. 110 (1999) 2822.
[53] F.B. van Duijneveldt, J.G.C.M. van Duijneveldt de Rijdt, J.H. van Lenthe, Chem. Rev. 94 (1994) 1873.
[54] P.B. Armentrout, M.T. Rodgers, J. Phys. Chem. A 104 (2000) 2238.
[55] C.H.S. Wong, F.M. Siu, N.L. Ma, C.W. Tsang, THEOCHEM 588 (2002) 9.
[56] N.F. Dalleska, B.L. Tjelta, P.B. Armentrout, J. Phys. Chem. 98 (1994) 4191.
[57] J.C. Amicangelo, P.B. Armentrout, Int. J. Mass Spectrom. 212 (2001) 301.
[58] C.Y. Peng, H.B. Schlegel, Israel J. Chem. 33 (1994) 449.
[59] S.J. Suresh, V.M. Naik, J. Chem. Phys. 113 (2000) 9727.